T H E U N I V E R S I T Y O F M I C H I G A N

COLLEGE OF ENGINEERING
Department of Mechanical Engineering

Final Progress Report

PERFORMANCE COEFFICIENTS FOR POWERED WHEELS IN SAND

D. K. Kapur

Supervisor: E. T. Vincent

ORA Project 02860

under contract with:

DEPARTMENT OF THE ARMY
U. S. ARMY ORDNANCE CORPS
DETROIT ORDNANCE DISTRICT
CONTRACT NO. DA-20-018-ORD-18955
DETROIT, MICHIGAN

administered through:

OFFICE OF RESEARCH ADMINISTRATION ANN ARBOR

March 1962

LIST OF FIGURES

Figure

Figure

LIST OF FIGURES (Concluded)

Figure

NOMENCLATURE

R	Horizontal component of the total force on the wheel—lb.
T	Wheel torque—in.-lb.
Z	Wheel sinkage—in.
d	Wheel diameter—in.
α	Wheel aspect ratio—nondimensional.
μ	Coefficient of friction (soil to wheel)—nondimensional.
D	Soil bed depth—in.
W	Wheel load—lb.
i	Wheel slip—nondimensional.
k_ϕ	Sinkage modulus (frictional)—$lb/in.^{n+2}$.
k_c	Sinkage modulus (cohesive)—$lb/in.^{n+1}$.
n	Sinkage index—nondimensional.
ω	Angular velocity of the wheel.
V_w	Tangential velocity of surface of wheel.
V_c	Linear horizontal velocity of wheel.
I	Instantaneous center of rotation.

ABSTRACT

This report covers experimental results obtained to demonstrate the usefulness of similitude studies for soil-vehicle analysis work when employing rigid powered wheels in a friction material such as dry sand.

A range of load coefficients, wheel diameters, aspect ratios, and wheel slip from -100 to +100% were covered in the tests. Satisfactory dimensionless parameters existed over the range of sizes covered for load, sinkage, torque, and draw-bar coefficients.

I. INTRODUCTION

The method of dimensional analysis and the technique of similitude testing have been increasingly used during the past two decades to predict the nature of a variety of physical phenomena. The advantages of scale-model testing over full-scale testing are many. Major gains are realized in economy, measurement accuracy, and the precise control of test conditions. The results of dimensional analysis provide a means for correlating and scaling the experimental data obtained from model tests.

Dimensional analysis differs from other types of analysis in that it is based solely on the relationships that must exist among pertinent variables because of their dimensions. In itself, dimensional analysis gives qualitative rather than quantitative relationships. When combined with experimental procedures, however, it may be made to supply quantitative results and accurate prediction equations.

The major shortcoming of dimensional analysis is its inability to produce a complete mathematical solution which describes a particular phenomenon. It sheds little light on the detailed physical mechanism involved. Dimensional analysis will, however, produce the information necessary to describe a particular phenomenon by means of a dimensionally correct equation.

The initial step in applying the method of dimensional analysis is to list the basic variables involved which might possibly be influential in the particular problem. These variables are then grouped to give a number of dimensionless products which are termed "master variables."

Langhaar[1] has shown that a particular relationship exi
ber of master variables in terms of the number of basic variables and basic dimensions. If N is the total number of basic variables involved, and γ is the rank of the dimensional matrix of the N variables, then the number of master variables is given by $(N-\gamma)$. One of these master variables, which generally contains the dependent basic variable, will in itself be dependent and the remainder will be independent.

II. THE APPLICATION OF THE METHOD OF DIMENSIONAL ANALYSIS TO POWERED WHEELS OPERATING IN A NONCOHESIVE SOIL

Of paramount importance in applying the method of dimensional analysis to a physical problem is the determination of those variables which are influential in describing the system. In the instance of a rigid powered wheel operating in a deformable soil, the use of the Bekker[2] soil value system leads to the following test variables.

Dependent Variables

R	horizontal component of the total force on the wheel—(lb.)
Z	wheel sinkage—(in.)
T	wheel torque—(in.-lb.)

Independent Variables

d	wheel diameter—(in.)
α	wheel aspect ratio—(nondimensional)
μ	coefficient of friction—soil-to-wheel (nondimensional)
D	soil bed depth—(in.)
W	wheel load—(lb.)
i	wheel slip—(nondimensional)
k_ϕ	sinkage modulus—(frictional)—$lb./(in.)^{n+2}$
k_c	sinkage modulus—(cohesive)—$lb./(in.)^{n+1}$
n	sinkage index—(nondimensional)

The dependent variables R, Z, and T are unknown functions of the independent variables listed previously. This may be expressed functionally as:

$$R = f_1(d,\alpha,\mu,D,W,i,k_\phi,k_c,n) \tag{1a}$$

$$Z = f_2(d,\alpha,\mu,D,W,i,k_\phi,k_c,n) \tag{1b}$$

$$T = f_3(d,\alpha,\mu,D,W,i,k_\phi,k_c,n) \tag{1c}$$

Each of the above unknown functional relationships involves ten variables. An analysis of the dimensionless matrix of these variables, using the M, L, T system of units reveals the rank of the matrix to be of order 2. As a consequence of Langhaar's rule, the number of master variables which can be formed for each equation is 10-2 or 8.

The dimensionless master variables are found by a method attributed to

Lord Rayleigh. Equation (1a) can be written as:

$$\frac{R}{W} = (W)^{a_1} \cdot (D)^{a_2} \cdot (d)^{a_3} \cdot (i)^{a_4} \cdot (\mu)^{a_5} \cdot (n)^{a_6} \cdot (k_\phi)^{a_7} \cdot (k_c)^{a_8} \cdot (\alpha)^{a_9} \tag{2}$$

In this expression the exponents are arbitrary constants. In dimensional form Eq. (2) becomes:

$$0 = (MLT^{-2})^{a_1} \cdot (L)^{a_2} \cdot (L)^{a_3} \cdot (ML^{-(n+1)} \cdot T^{-2})^{a_7} \cdot (ML^{-n} T^{-2})^{a_8} \tag{3}$$

Equating the exponents of M, L, and T, produces:

$$a_1 + a_7 + a_8 = 0$$

$$a_1 + a_2 + a_3 - (n+1)a_7 - n\, a_8 = 0$$

Expressing a_8 and a_7 in terms of a_1, a_2 and a_8 yields:

$$a_3 = -(n+2)a_1 - a_2 - a_8$$

$$a_7 = -a_1 - a_8$$

The substitution of a_3 and a_7 in Eq. (2) with subsequent simplification produces the following expressions for the master variables:

$$\frac{R}{W} = (W)^{a_1}(D)^{a_2}(d)^{-(n+2)a_1-a_2-a_8} \cdot (i)^{a_4} \cdot (\mu)^{a_5} \cdot (n)^{a_6} \cdot (k_\phi)^{-a_1-a_8} \cdot (k_c)^{a_8}(\alpha)^{a_9}$$

$$\frac{R}{W} = \left(\frac{W}{d^{n+2} \cdot k_\phi}\right)^{a_1} \cdot \left(\frac{D}{d}\right)^{a_2} \cdot (i)^{a_4}(\mu)^{a_5}(n)^{a_6} \cdot \left(\frac{k_c}{dk_\phi}\right)^{a_8}(\alpha)^{a_9} \tag{4}$$

A similar procedure is followed for expressing the dependent master variables, T/Wd, and Z/d in terms of the same independent dimensionless variables as R/W. Consequently the functional relations can be written as:

$$\left(\frac{R}{W}\right) = f_1\left\{\left(\frac{W}{d^{n+2}k_\phi}\right), \left(\frac{k_c}{dk_\phi}\right), \left(\frac{D}{d}\right), (\alpha), (\mu), (n), (i)\right\} \quad (5a)$$

$$\left(\frac{T}{Wd}\right) = \left\{\left(\frac{W}{d^{n+2}k_\phi}\right), \left(\frac{k_c}{dk_\phi}\right), \left(\frac{D}{d}\right), (\alpha), (\mu), (n), (i)\right\} \quad (5b)$$

$$\left(\frac{Z}{d}\right) = \left\{\left(\frac{W}{d^{n+2}k_\phi}\right), \left(\frac{k_c}{dk_\phi}\right), \left(\frac{D}{d}\right), (\alpha), (\mu), (n), (i)\right\} \quad (5c)$$

Complete similitude then requires that the following conditions be met:

$$\left(\frac{W}{d^{n+2}k_\phi}\right)_p = \left(\frac{W}{d^{n+2}k_\phi}\right)_m \quad (6a)$$

$$\left(\frac{k_c}{dk_\phi}\right)_p = \left(\frac{k_c}{dk_\phi}\right)_m \quad (6b)$$

$$\left(\frac{D}{d}\right)_p = \left(\frac{D}{d}\right)_m \quad (6c)$$

$$(\alpha)_p = (\alpha)_m \quad (6d)$$

$$(\mu)_p = (\mu)_m \quad (6e)$$

$$(n)_p = (n)_m \quad (6f)$$

$$(i)_p = (i)_m \quad (6g)$$

In the above similarity conditions the subscripts m and p respectively stand for model and prototype. A simplification of these conditions occurs if the same soil is used in both the prototype and the model testing. For sand the cohesive modulus is zero. As a consequence the conditions necessary for similitude in the problem being investigated reduce to:

$$\left(\frac{W}{d^{n+2}k_\phi}\right)_p = \left(\frac{W}{d^{n+2}k_\phi}\right)_m \quad (7a)$$

$$\left(\frac{D}{d}\right)_p = \left(\frac{D}{d}\right)_m \quad (7b)$$

$$(\alpha)_m = (\alpha)_p \tag{7c}$$

$$(i)_m = (i)_p \tag{7d}$$

III. EXPERIMENTAL RESEARCH

An experimental investigation was conducted to verify the validity of the foregoing similitude parameters for the powered rigid wheels in sand. The investigation utilized rigid smooth aluminum wheels of rectangular cross-section operating in dry beach sand. Tests were conducted using a 12.5-in. diameter wheel and an 8.56-in. diameter wheel, both of which had an aspect ratio of 0.52.

Tests were also conducted to explore the effect of aspect ratio on the dependent variables R, T, and Z for the larger 12.5-in. diameter wheel. For the selected wheel diameter d, the sand bed depth D, aspect ratio α, and wheel load W were varied in accordance with the requirements of similitude as expressed by Eqs. (7a-d). The particular values selected and their range are summarized in the chart below. The dependent variables, R, T, and Z were measured for each individual test.

Wheel Diameter (in.)	Aspect Ratio	Wheel Load (lb.)	Bed Depth (in.)
12.50	0.27	10,20,40 60 & 100	8.0
12.50	0.52		
12.50	0.84		
8.56	0.52	3.25,6.50,13.0 20 & 33	5.5

The beach sand used during the tests has an average set of properties characterized by $k_c = 0$, $k_\phi = 3.4$ and $n = 1.05$. The wheel slip was independently varied from a -100% to a +100%. In this program the slip is computed as:

$$i = \left(\frac{\vec{V}_w - \vec{V}_c}{\vec{V}_c} \right)$$

where

V_w = Tangetial velocity of surface of wheel,

and

V_c = Linear horizontal velocity of wheel.

Figure 1 shows the assigned directions for positive torque and net horizontal force exerted by the sand on the wheel. It also shows the positive directions of linear and angular velocities.

APPARATUS

The equipment employed in the research is described in detail in Ref. 4, with the exception that, for the tests under discussion, the wheel was driven by an electric motor, trunnion-mounted for torque reaction measurements to record both torque and power inputs when necessary.

The wheel-carrying assembly had been modified somewhat to accommodate the components required for driving the wheel. The drive motor, speed reducer, and the power source (batteries) were all mounted on the test carriage. A detail view of the wheel-carrying assembly is shown in Fig. 5, where it is seen that the wheel is now mounted on a counterbalanced beam which can be loaded by the addition of weights over the wheel axle. The beam is kept horizontal by the the vertical adjustment of the complete carriage, described in previous report.

IV. RESULTS AND DISCUSSION

A dimensional equation expresses a certain unknown functional relationship between the measured (dependent) master variables and a number of fixed (independent) master variables. If the functional relationship between all of the master variables were specifically known, the solution would be unique when all pertinent variables of the system are included in the analysis. Experimental studies with scale models enables a direct verification of a set of dimensional equations describing a particular physical problem. Verification is accomplished by conducting two or more different tests with scale models under conditions such that values of independent master variables remain unaltered. Under these test conditions the measured values of all the dependent master variables should be the same for the range of test conditions.

The dimensionless parameters obtained from the experimental measurements made on powered rigid wheels operating in sand are shown in Fig. 5 through 20. These Figures present the values of the measured master variables R/W (Figs. 6-10), T/Wd (Figs. 11-15), and Z/d (Figs. 16-20), for two different test conditions which satisfy the similarity requirements of Eqs. (7a-d). These figures all display a marked degree of similitude, thus attesting to the validity of the selected dimensional parameters for powered rigid wheels in frictional soils. (For towed wheels see Ref. 3.) Figures 6 and 7 at low load coefficients show some scatter in the observations, but here the equipment is operating with forces so small that the sensitivity of the measuring devices is approached.

Figures 21 through 35 indicate the effect of varying aspect ratio, α, on the various dependent master variables. The occurrence of negative values of the motion resistance R indicate the development of a net tractive effort by the wheel. The net tractive effort of a wheel is often characterized by a quantity known as the draw-bar pull. The draw-bar pull is defined as the difference between the gross traction force produced by the shearing strength of the soil and the motion resistance of the wheel. The variation of draw-bar pull for a range of slips, load coefficients, and aspect ratios is presented in Figs. 26 through 31.

Draw-bar pull (DP) and the dimensionless ratio DP/W for a slip of +25% are shown as a function of load coefficient in Figs. 36 and 37. These figures are typical of the results obtained and the tests display the following characteristics:

(1) DP/W decreases with increasing load W for all values of α.

(2) DP/W increases with increasing α for the same load.

(3) DP/W increases with increasing positive slip up to about 25%. Above this value it remains essentially constant.

(4) DP increases with increasing loads initially and then begins to decrease ultimately reaching a negative value.

(5) DP/W and DP are positive for a narrow range of load coefficient, especially for low aspect ratios.

(6) Aspect ratio has a pronounced effect on R/W and Z/d, and almost negligible on T/Wd.

(7) T/Wd approaches a constants value of 0.24 for large positive slip, irrespective of wheel diameter and aspect ratio, for all load coefficients.

In frictional soils the gross traction developed varies directly with load and is independent of the area of contact of wheel to soil. From the results presented in Fig. 37, it is seen that motion resistance decreases with increasing α for the same load and wheel diameter.

FUTURE ANALYSIS

The data accumulated in these tests present possible solutions to many problems and much further analysis is required to draw all possible data from these results. It is proposed to carry on this work as occasion permits.

APPENDIX

SOIL REACTIONS AGAINST DRIVEN WHEELS

Consider a hard smooth circular wheel driven on deformable ground (Fig. 2). The wheel is rotating about the center of the axle O with constant angular velocity w in clockwise direction. Also the wheel has a linear velocity V_c parallel to the surface of undisturbed ground level (UGL). Let V_w be the tangential velocity of the surface of the wheel with respect to O.

Knowing the magnitudes of V_c and V_w, the instantaneous center of rotation I can be located. For all relative magnitudes of V_c and V_w, the instantaneous center remains in a vertical plane through the axis of rotation of the wheel and perpendicular to the plane of paper. Its position depends on the difference in magnitudes of V_c and V_w. For different values of V_w and V_c the location of I is illustrated in Fig. 3. Taking a general case (Fig. 2), let V_c and V_w be such that I is located between O and C and below the UGL. An interesting division of the wheel into four parts can be made by two planes: (i), a plane passing through OC and perpendicular to the plane of paper; and (ii), a plane through AIB and perpendicular to the plane of paper.

All points of the wheel in the plane through AIB have no motion parallel to the motion of the center of the axle O. All points below this plane have a backward motion with respect to ground, and all points above this plane have a forward motion with respect to ground. Again, all points in plane through OIC have no motion perpendicular to the motion of the center of the axle O. All points back of plane through OIC have an upward motion with respect to ground, and all the points in front of this plane have a downward motion with respect to ground. The relative motion of the points in four segments is shown by arrows included in dotted circles.

Thus, knowing the relative motion of the wheel segments with respect to ground, it is simpler to see how the ground offers reactions to the wheel. First of all, since the ground offers reactions to all those parts of the wheel which are in front of the plane through OIC and moving downwards, such as R, of Fig. 4, the resultant of these supporting ground reactions will lie somewhere between the plane through OIC and the foremost part of the wheel in contact with the ground. There is a resultant reaction R_2 on all those parts of the wheel which are back of plane through OIC, moving upwards, and in contact with the ground. The magnitude of R_2 is generally very small compared with R_1. R_2 probably will have a significant value if there were lugs on the surface of the wheel. These forces are shown in Fig. 4.

The soil offers tractive reactions against those parts of the wheel which

are below the plane through AIB and in contact with the ground. R_3, the resultant of all these reactions will lie somewhere between the plane through AIB and the lowest point of the wheel C. The resultant of all these reactions, R_4, lies between the plane through AIB and the highest point of contact of the wheel with the ground.

SOIL REACTIONS AT ZERO % SLIP

The zero percent slip for a hard wheel and a deformable ground is not as simple as it is for a hard wheel and hard ground. For the second case, when the hard wheel is moving over hard ground with zero slip, the instantaneous center is located on the line of contact of the two. As there is no relative motion, no resisting reactions are developed. The only force involved would be that of supporting reactions from ground due to the weight on the wheel plus those arising from elastic or similar deformations. But this is not the case for a hard wheel and deformable ground. The instantaneous center is still located at the same place on the wheel. Only those points of the wheel which lie on a line through I and parallel to the axis of rotation of the wheel have no relative motion with respect to ground. All other parts of the wheel, which are in contact with the ground have relative motion and this causes the resisting and tractive reactions.

REFERENCES

1. Langharr, H. L., Dimensional Analysis and Theory of Models, John Wiley and Sons, Inc., New York, 1951.

2. Bekker, M. G., Off-The-Road Locomotion, Univ. of Mich. Press, Ann Arbor, Mich., 1960.

3. Hicks, H. H., Jr., D. K. Kapur, and E. T. Vincent, A Similitude Study of the Drag and Sinkage of Wheels Using the Sinkage-Parameter System of Soil Values, UMRI Report 2860-27-P, Ann Arbor, Mich., April 1961.

4. Vincent, E. T., D. K. Kapur, and H. H. Hicks, Jr., Research in Vehicle Mobility, UMRI Report 2544-31-F, Ann Arbor, Mich., July 1960.

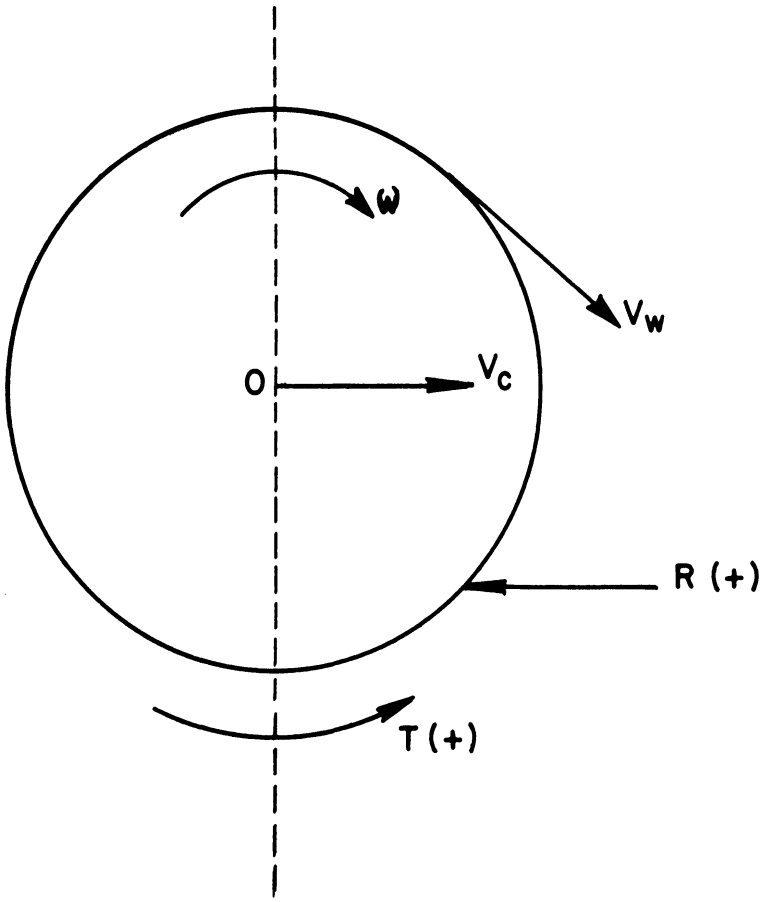

Fig. 1. Sign convention of velocities and forces on the wheel.

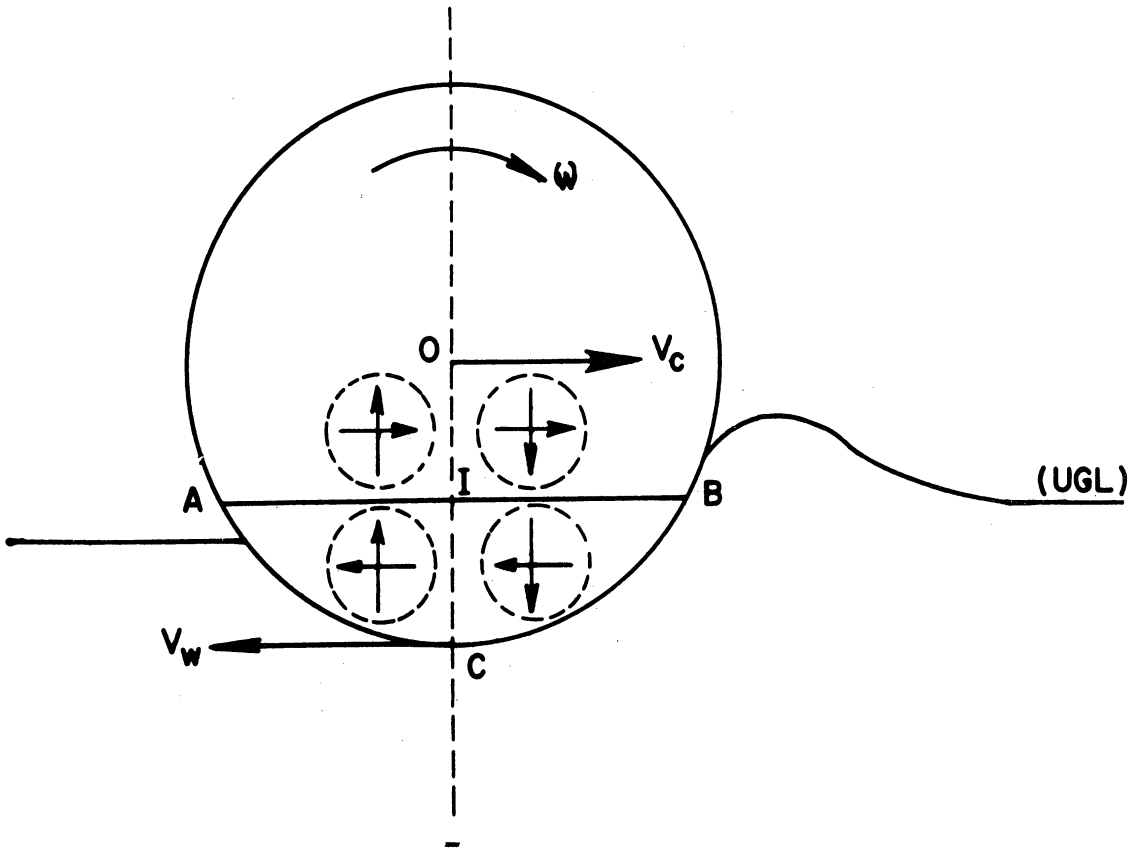

Fig. 2. Relative motion of different segments of wheel.

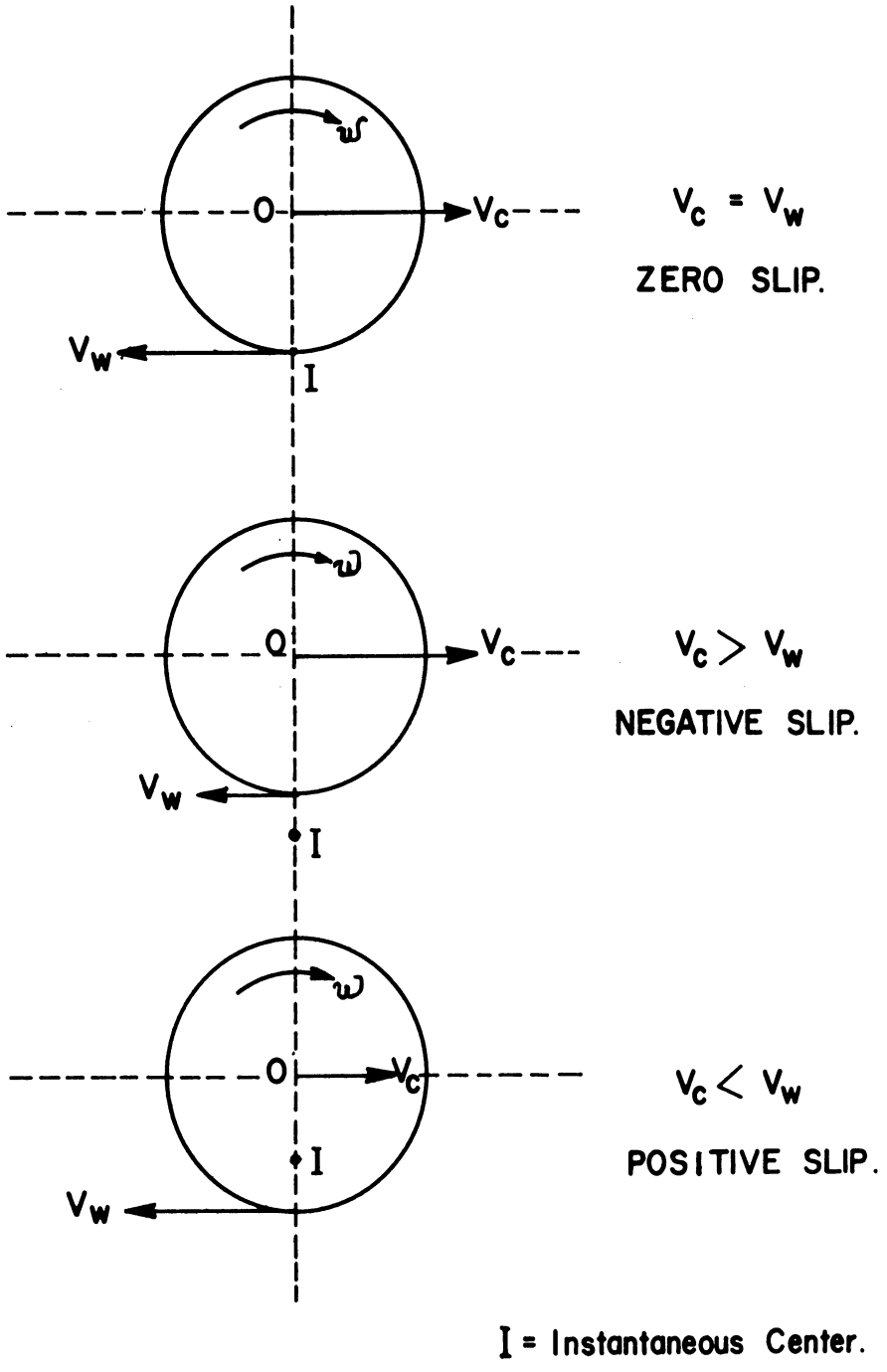

Fig. 3. Location of instantaneous center for different slips.

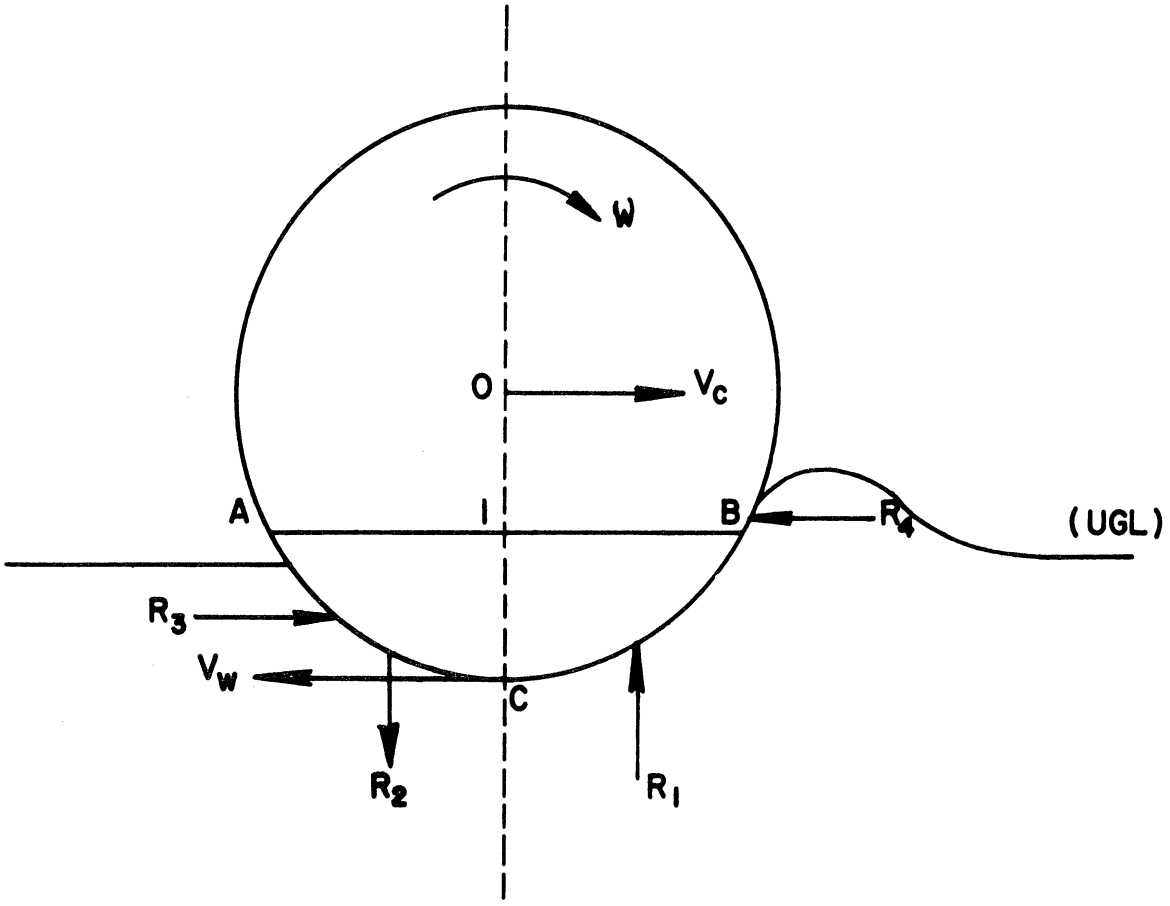

Fig. 4. Soil reactions on different parts of the wheel.

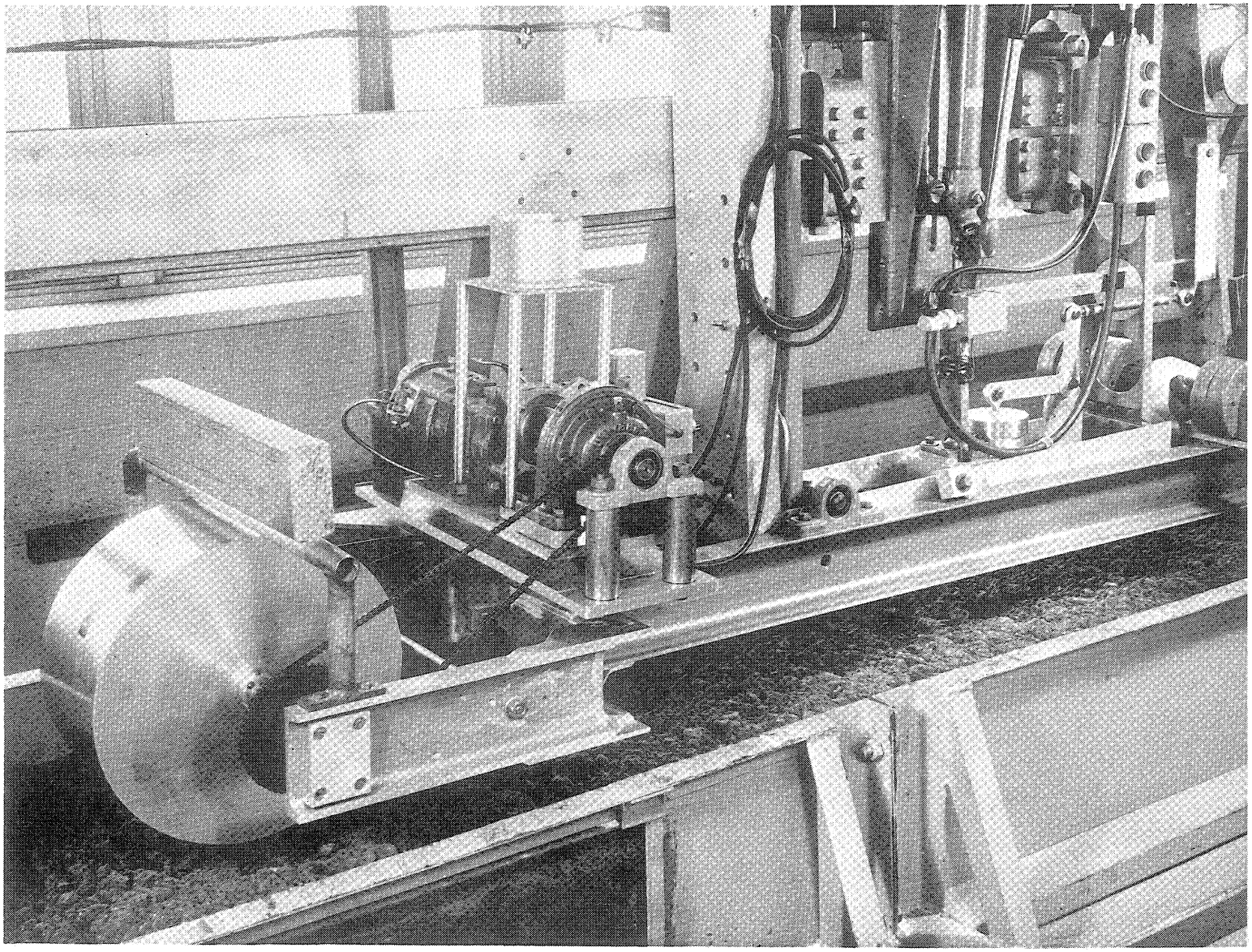

Fig. 5. Picture of wheel and motor drive.

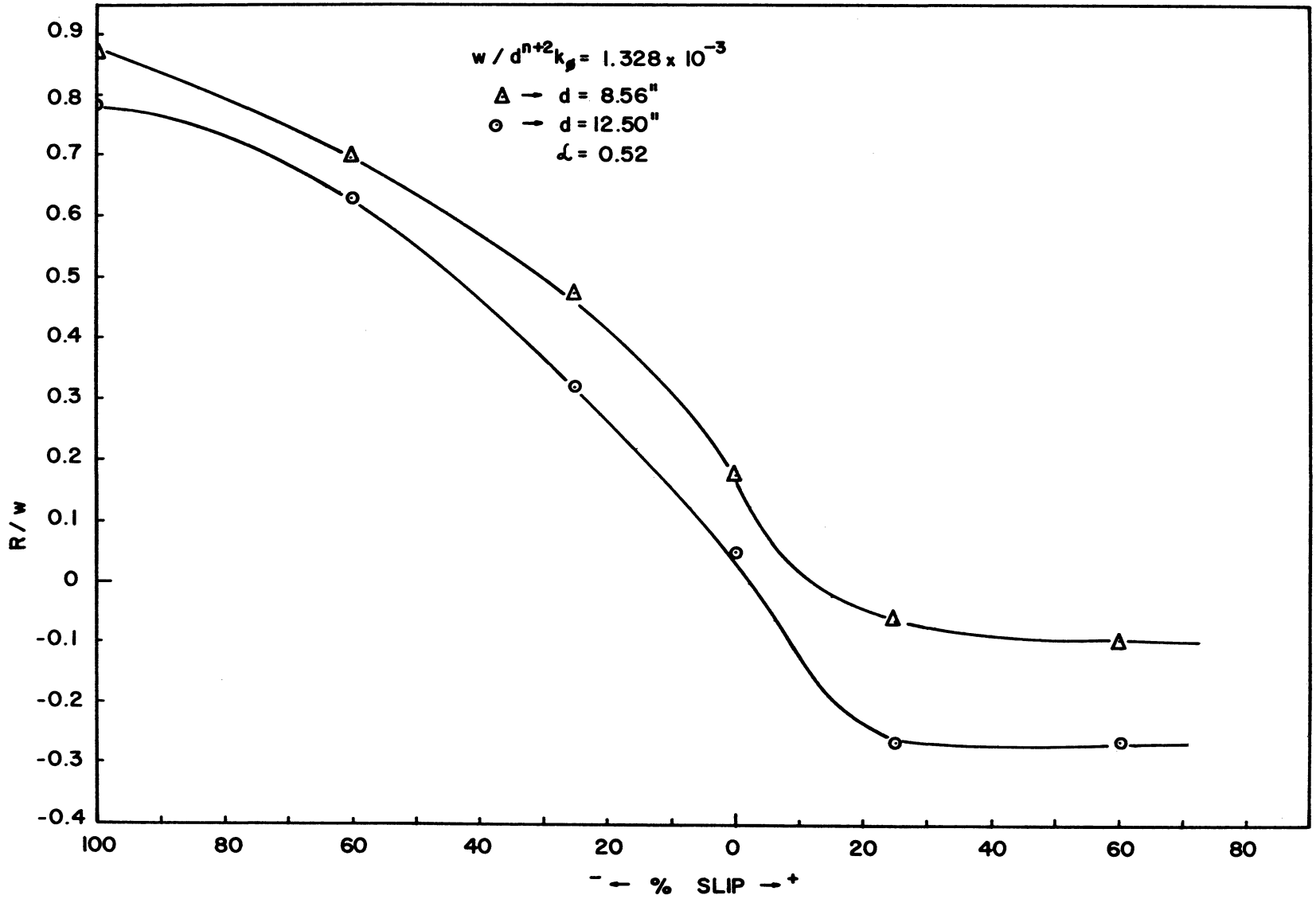

Fig. 6. Plot of (R/w) vs. % slip for ($w/d^{n+2}k_\phi = 1.328 \times 10^{-3}$) under similitude conditions.

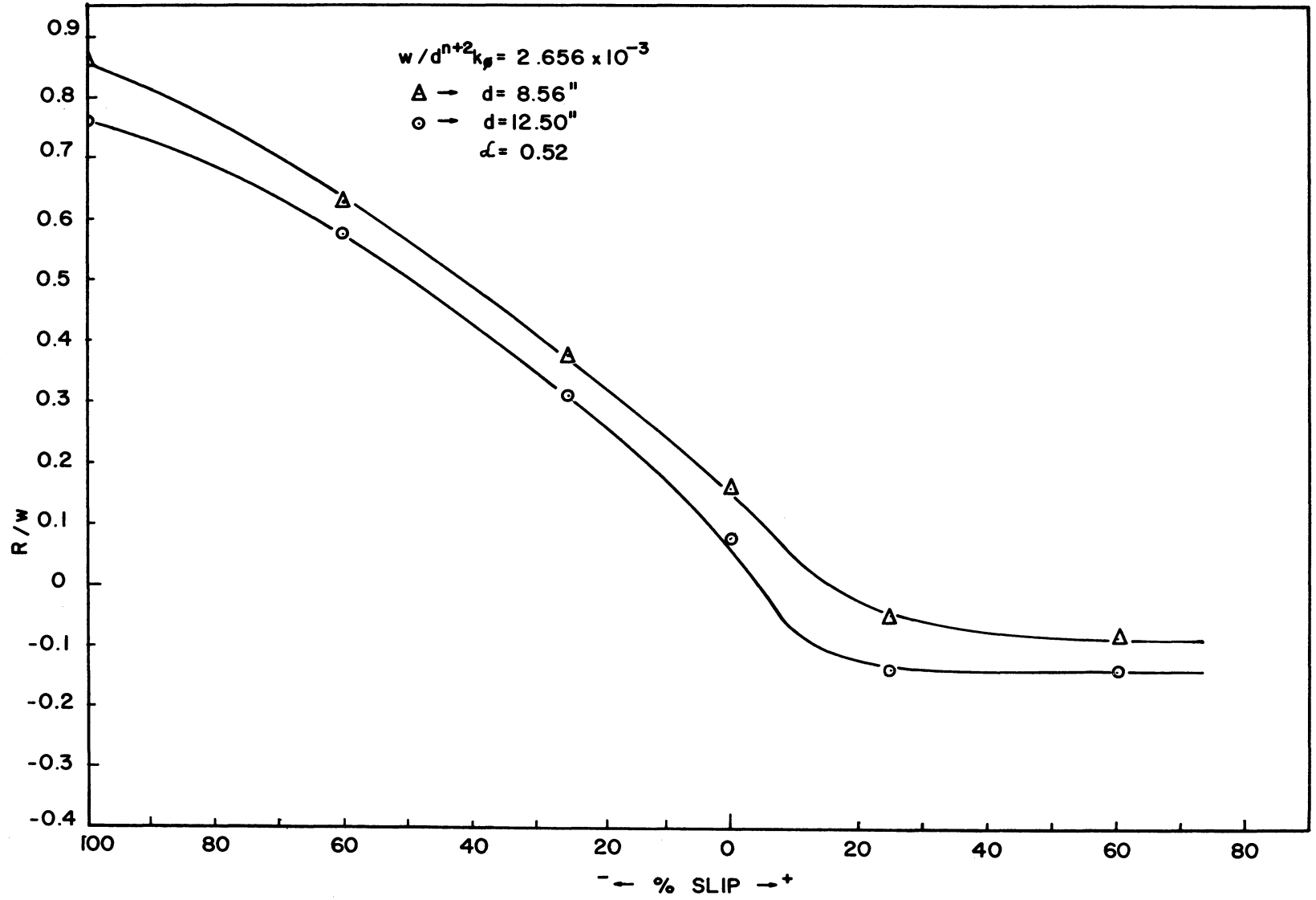

Fig. 7. Plot of (R/w) vs. % slip for ($w/d^{n+2}k_\phi = 2.656 \times 10^{-3}$) under similitude conditions.

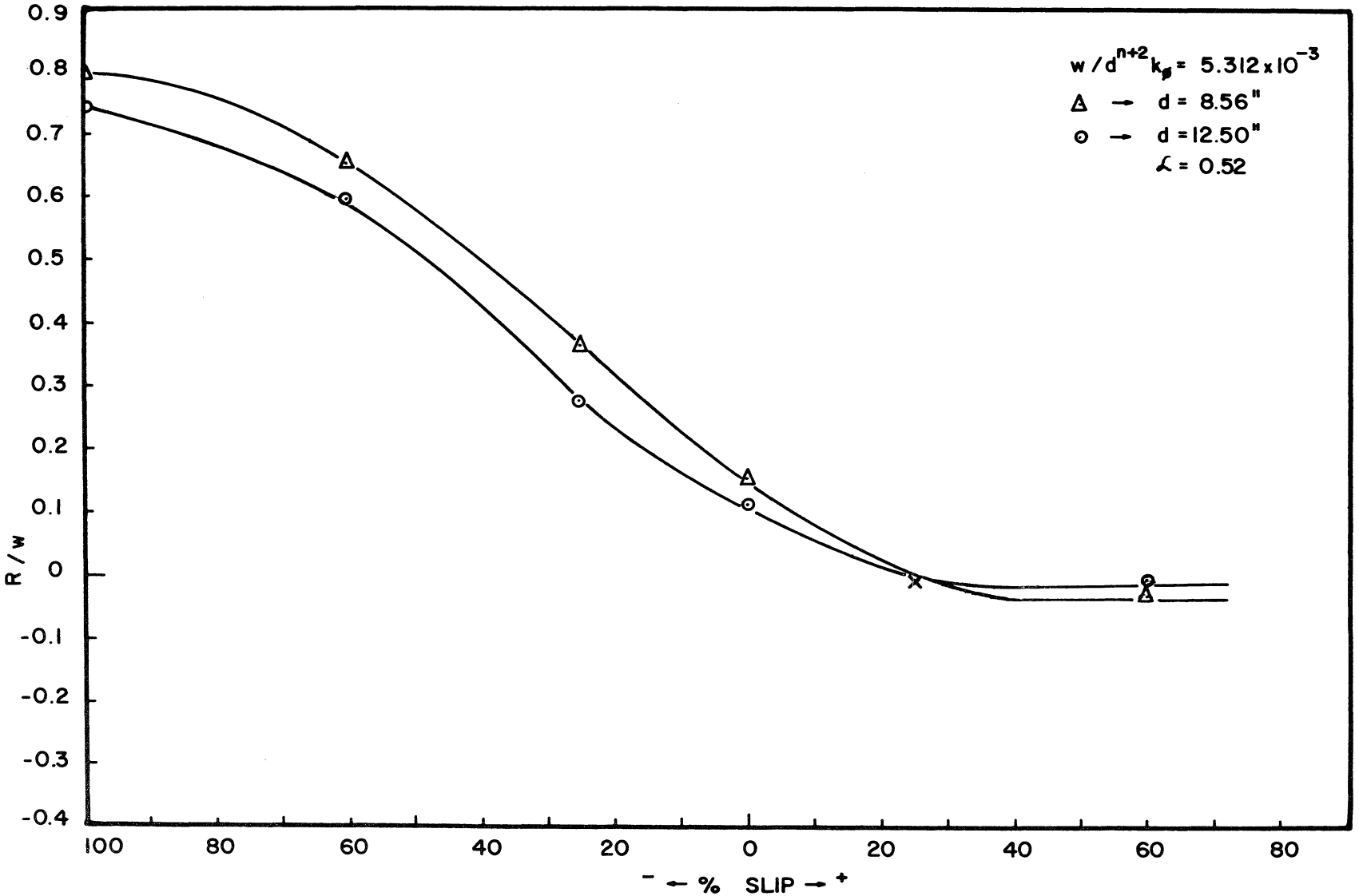

Fig. 8. Plot of (R/w) vs. % slip for ($w/d^{n+2}k_\phi = 5.312 \times 10^{-3}$) under similitude conditions.

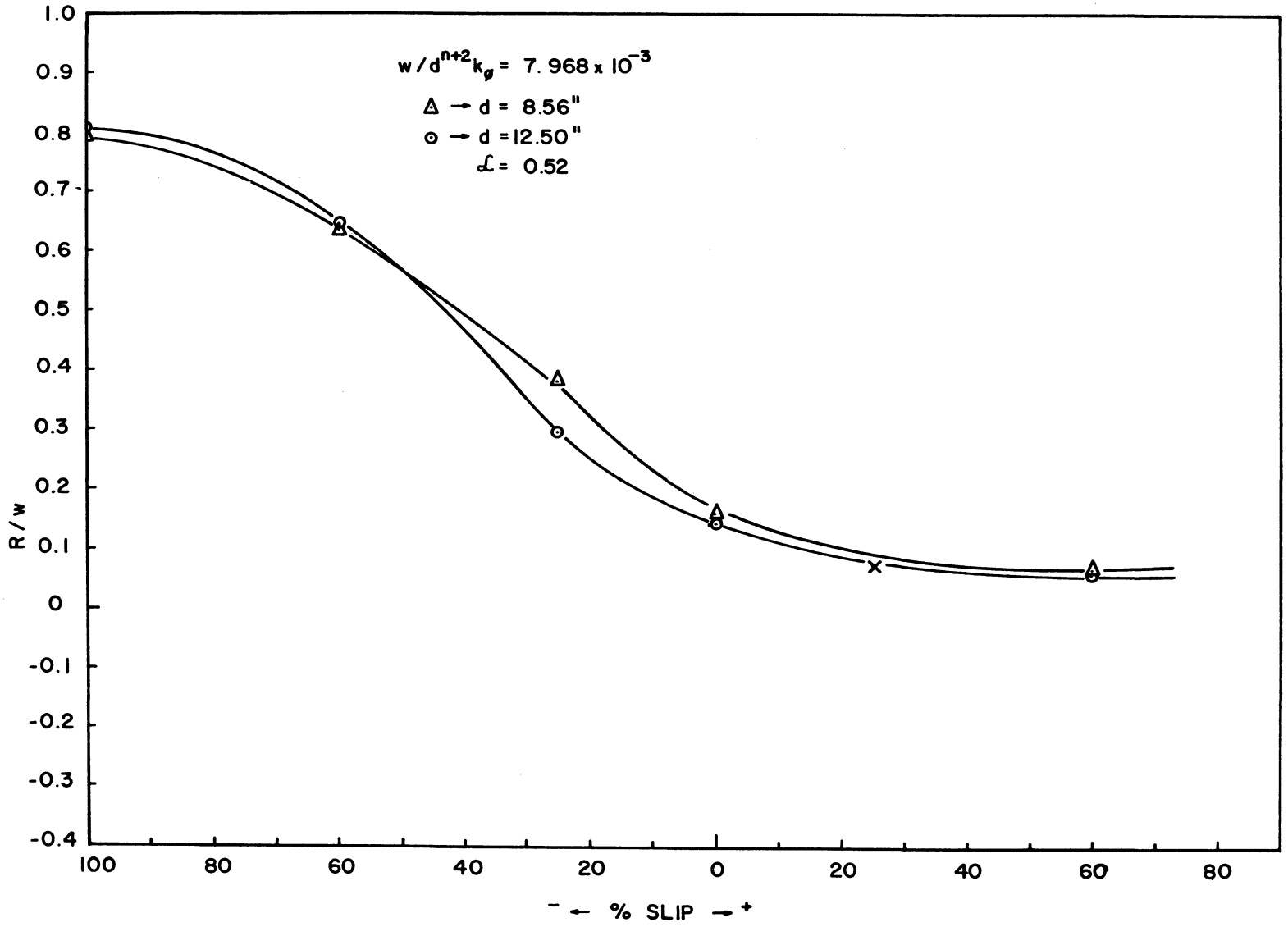

Fig. 9. Plot of (R/w) vs. % slip for $(w/d^{n+2}k_\phi = 7.968 \times 10^{-3}$ under similitude conditions.

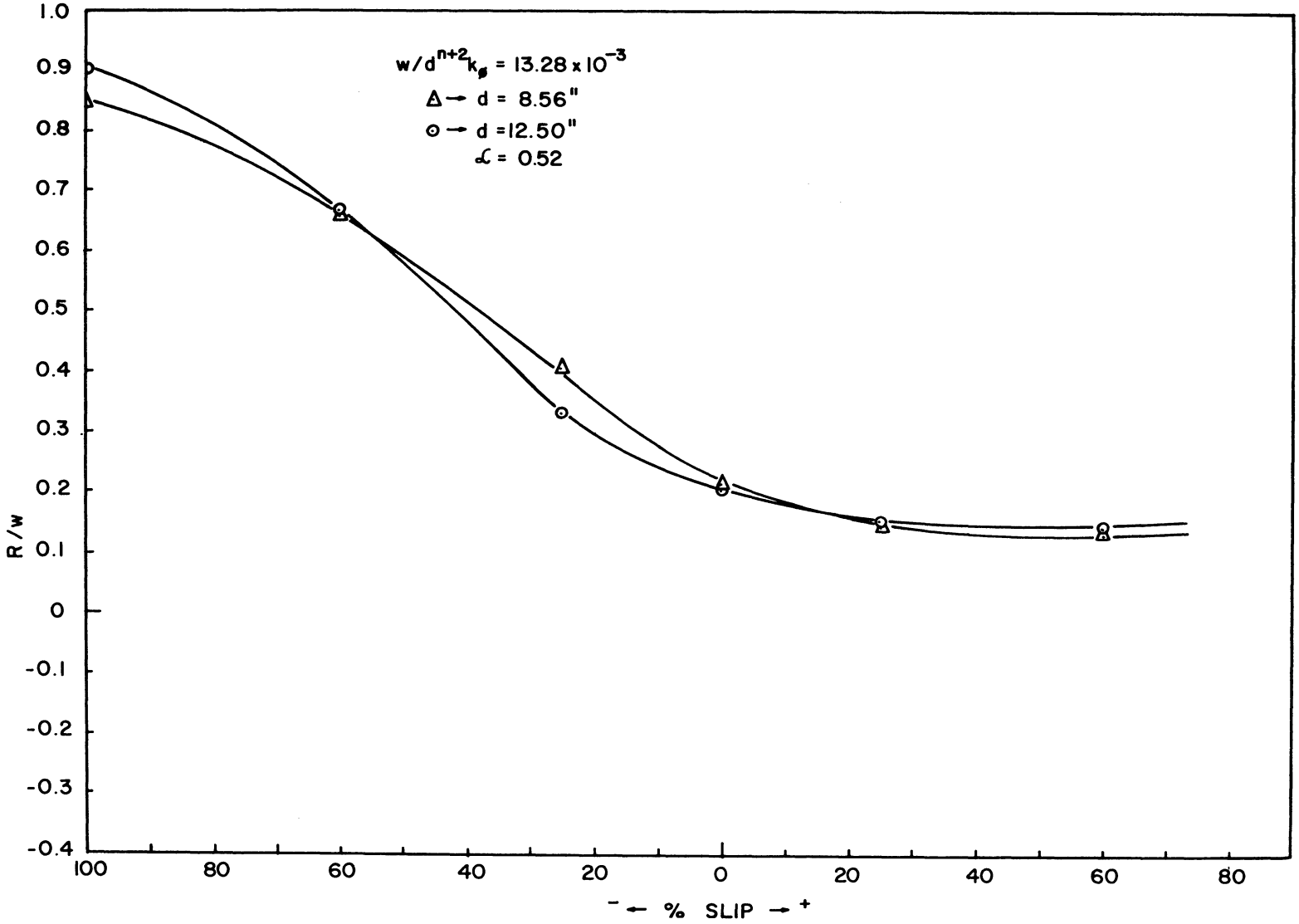

Fig. 10. Plot of (R/w) vs. % slip for ($w/d^{n+2}k_\phi = 13.28 \times 10^{-3}$) under similitude conditions.

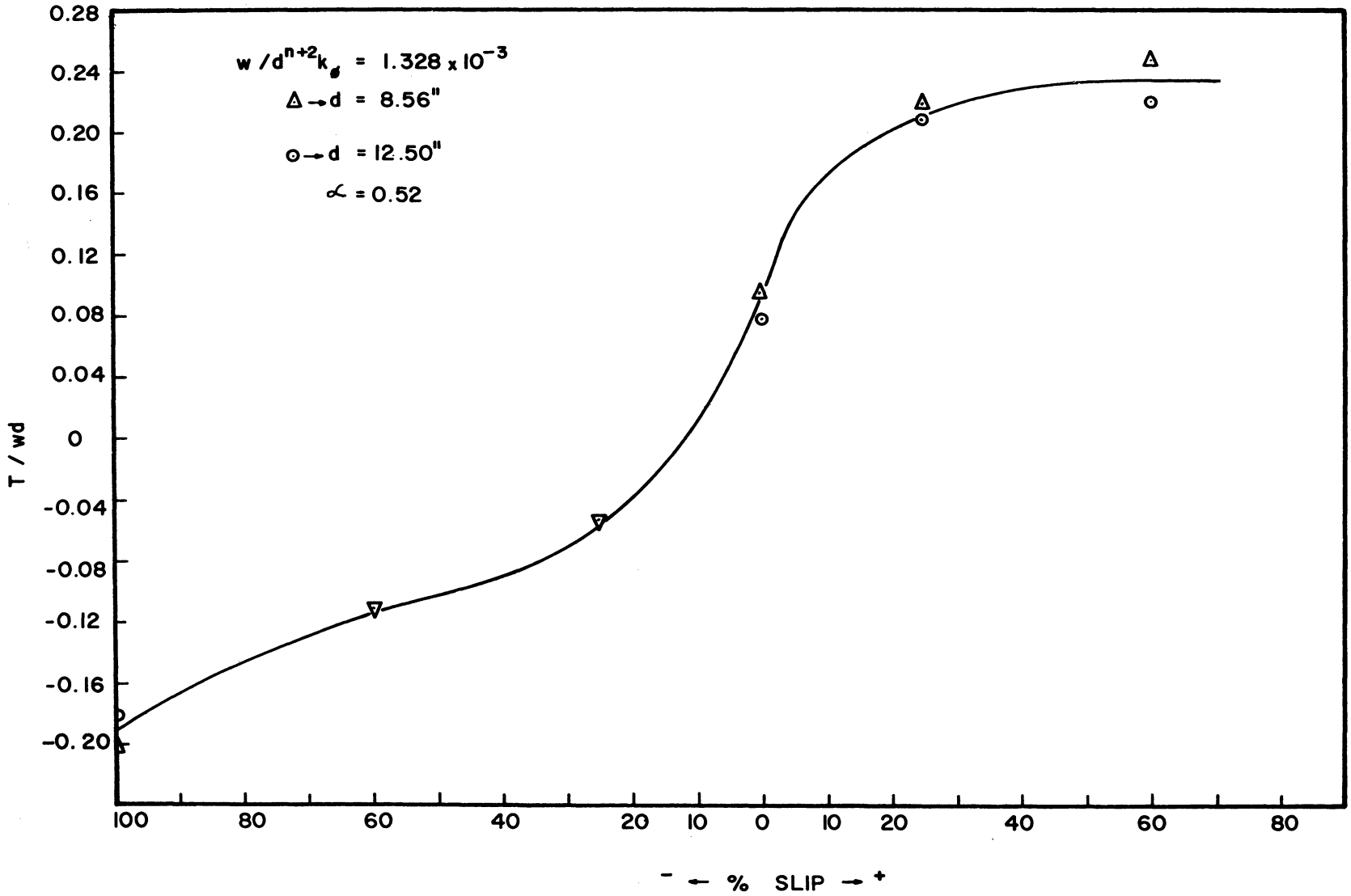

Fig. 11. Plot of (T/wd) vs. % slip for ($w/d^{n+2}k_\phi = 1.328 \times 10^{-3}$) under similitude conditions.

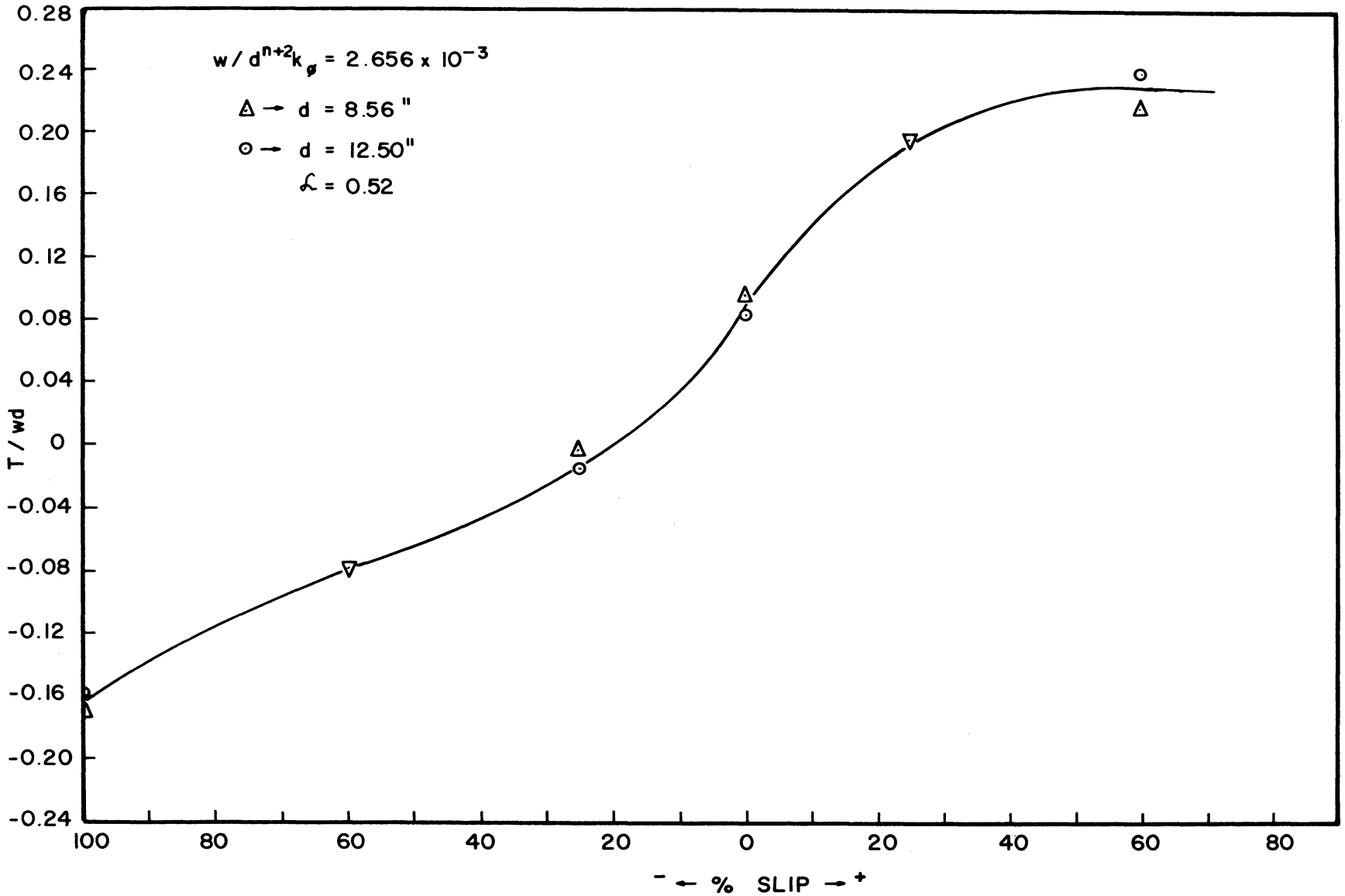

Fig. 12. Plot of (T/wd) vs. % slip for ($w/d^{n+2}k_{\phi} = 2.656 \times 10^{-3}$) under similitude conditions.

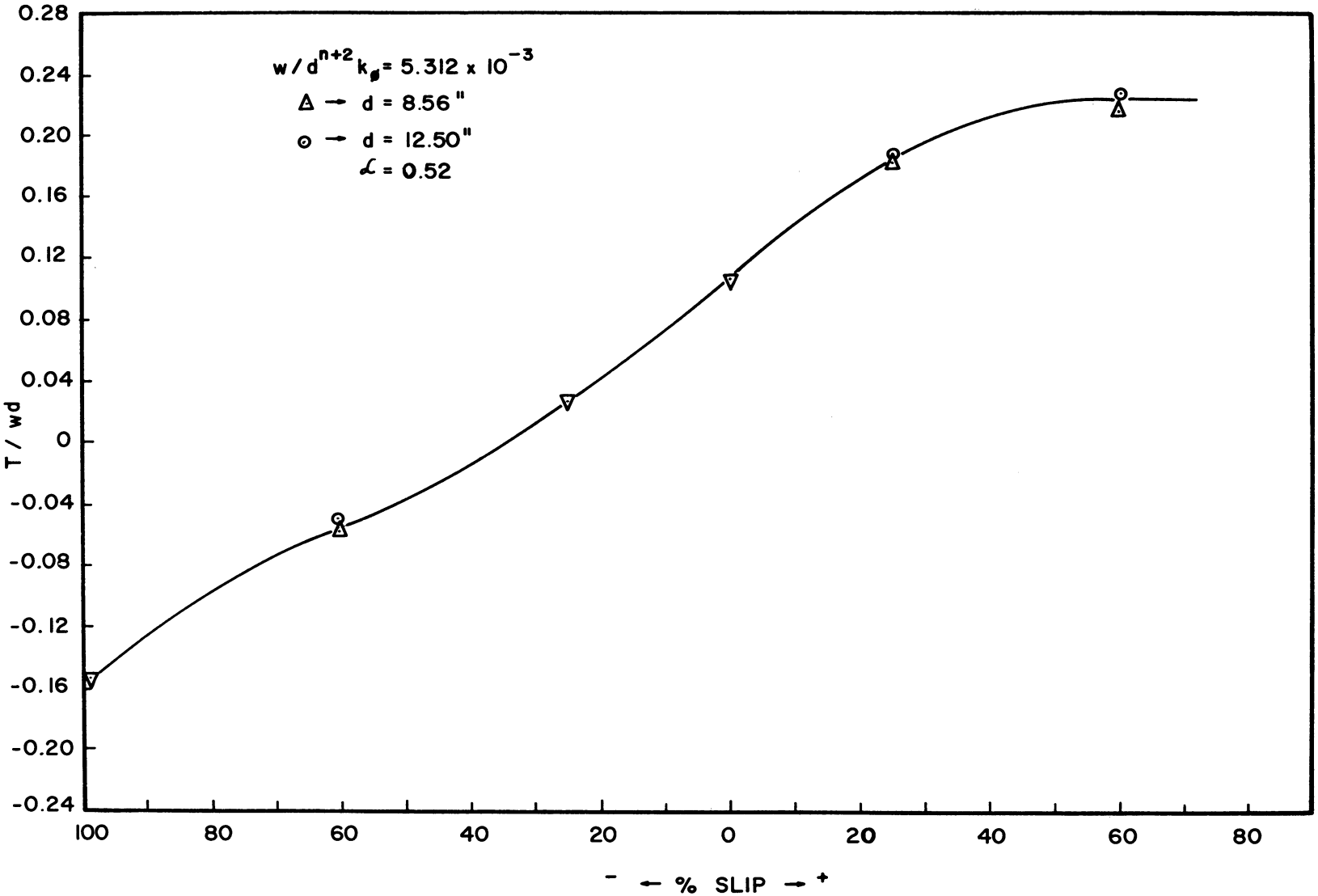

Fig. 13. Plot of (T/wd) vs. % slip for ($w/d^{n+2}k_\phi = 5.312 \times 10^{-3}$) under similitude conditions.

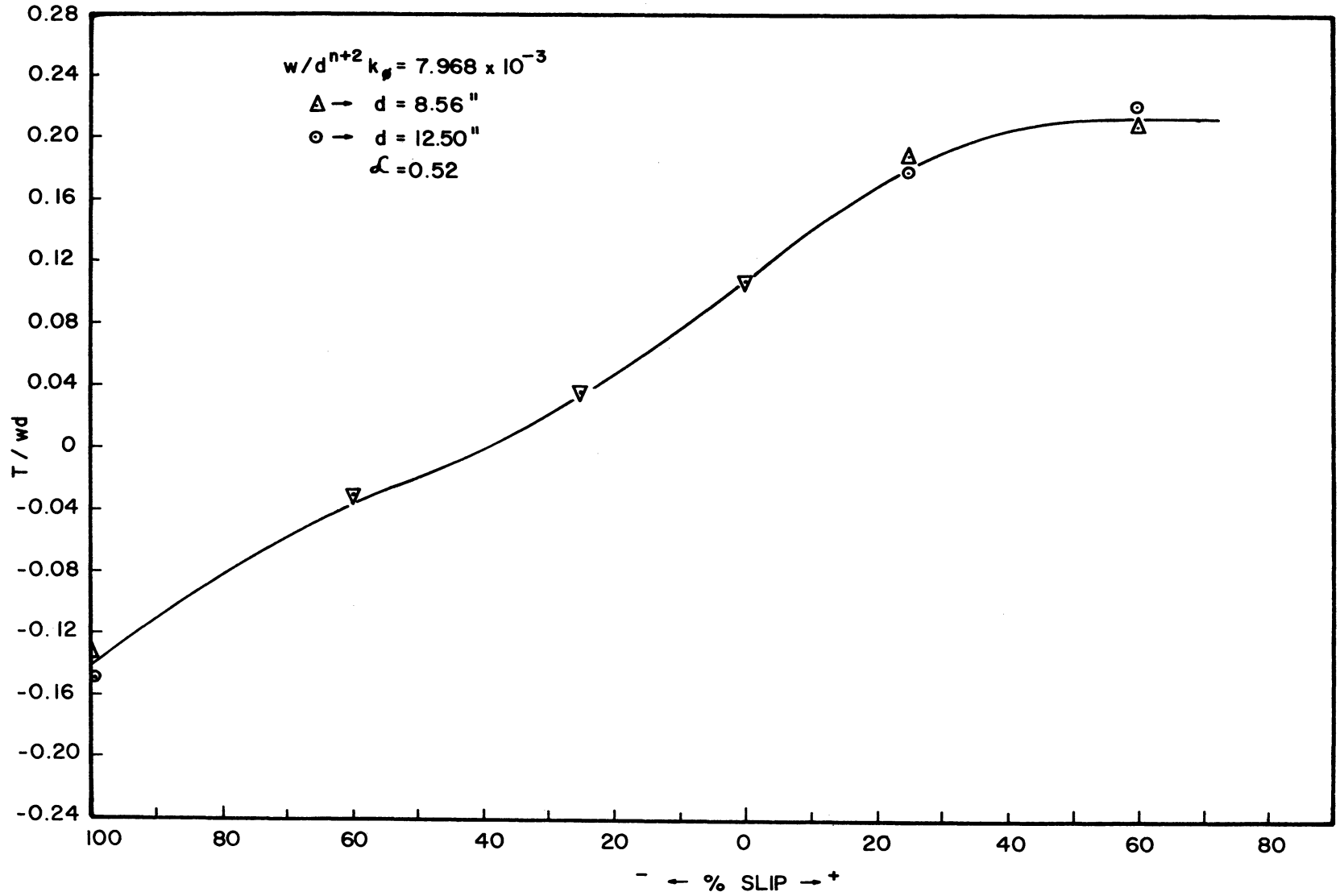

Fig. 14. Plot of (T/wd) vs. % slip for ($w/d^{n+2}k_\phi = 7.968 \times 10^{-3}$) under similitude conditions.

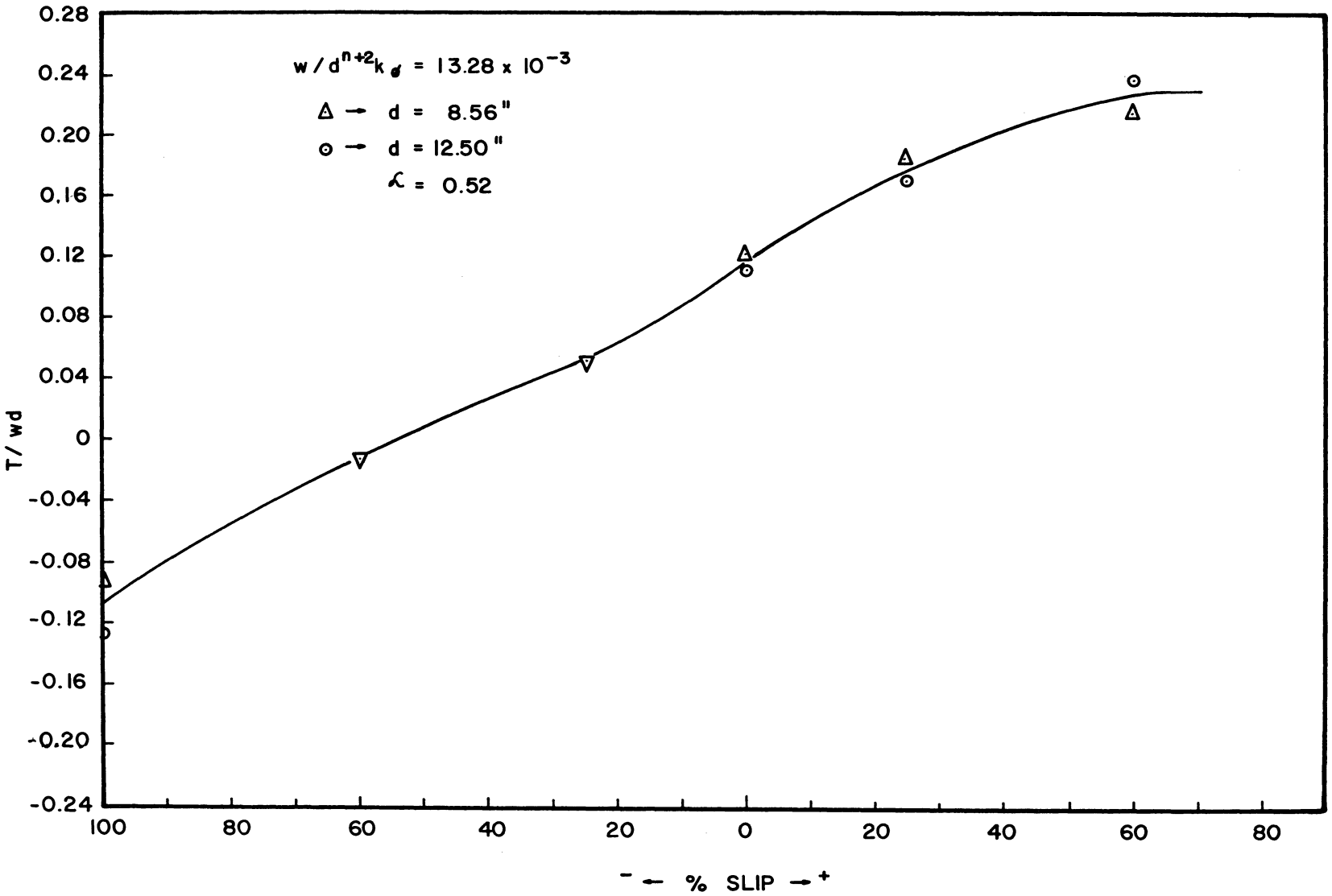

Fig. 15. Plot of (T/wd) vs. % slip for ($w/d^{n=2}k_\phi = 13.28 \times 10^{-3}$) under similitude conditions.

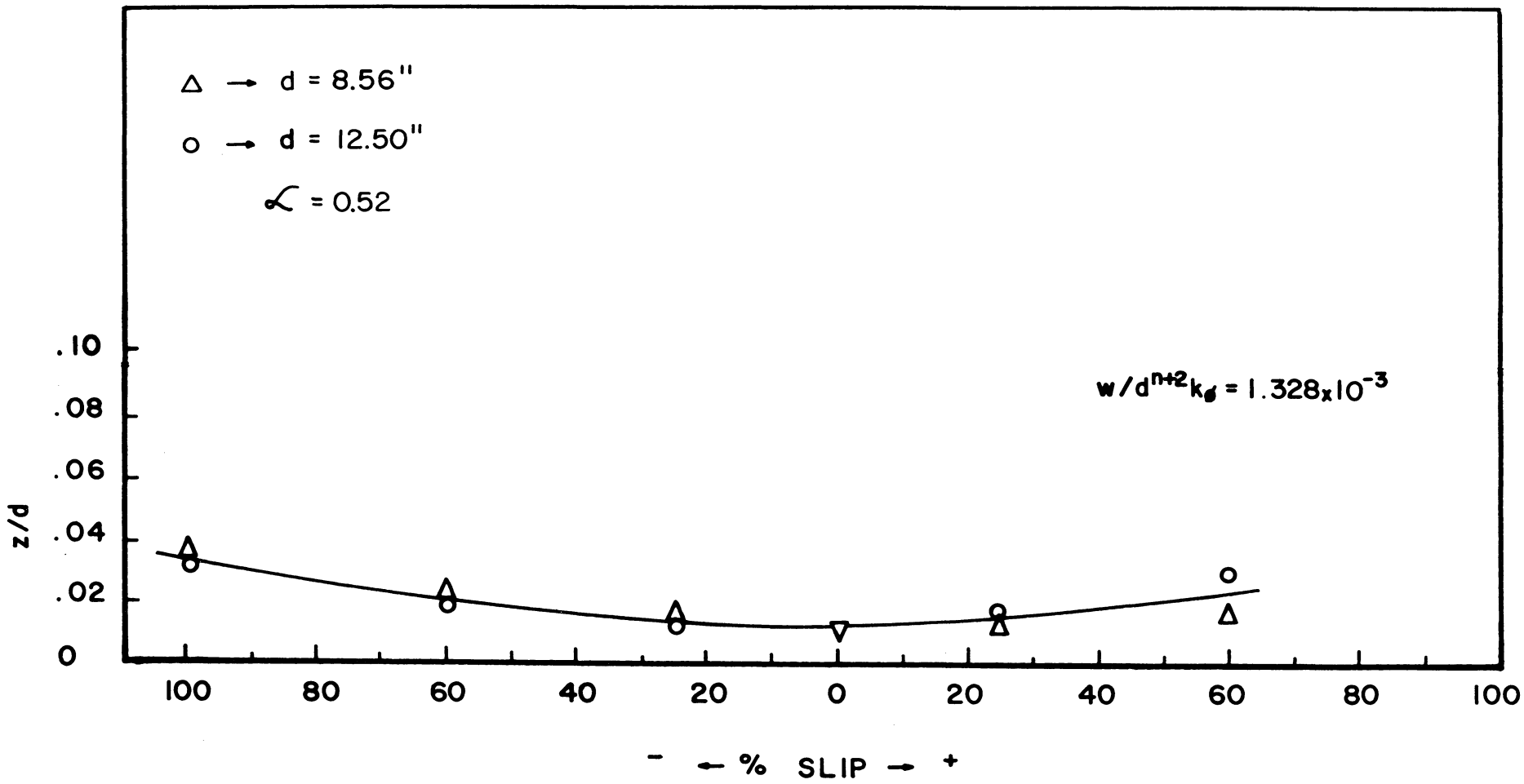

Fig. 16. Plot of (z/d) vs. % slip for ($w/d^{n+2}k_\phi = 1.328 \times 10^{-3}$) under similitude conditions.

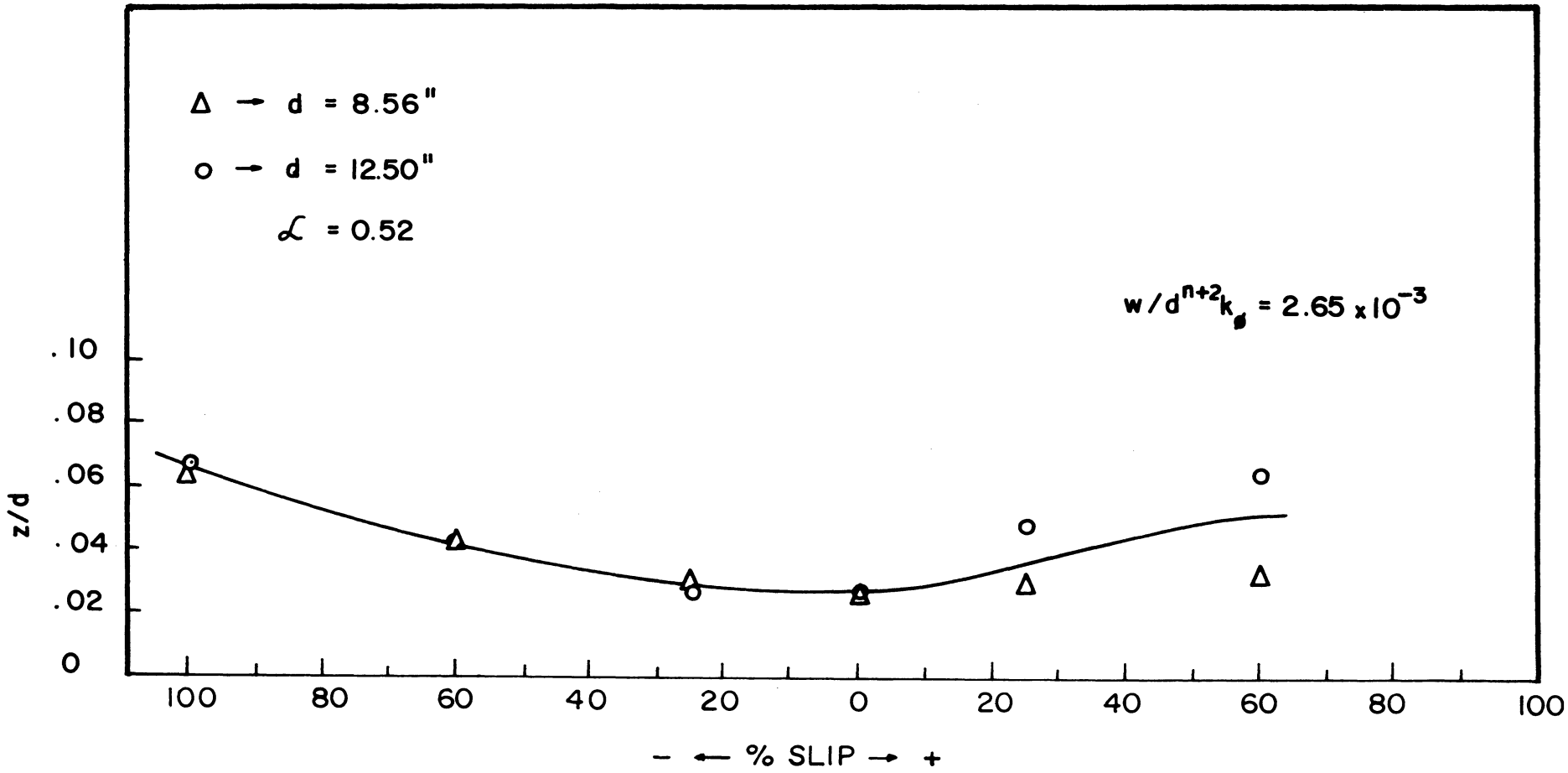

Fig. 17. Plot of (z/d) vs. % slip for ($w/d^{n+2}k_{\phi} = 2.656 \times 10^{-3}$) under similitude conditions.

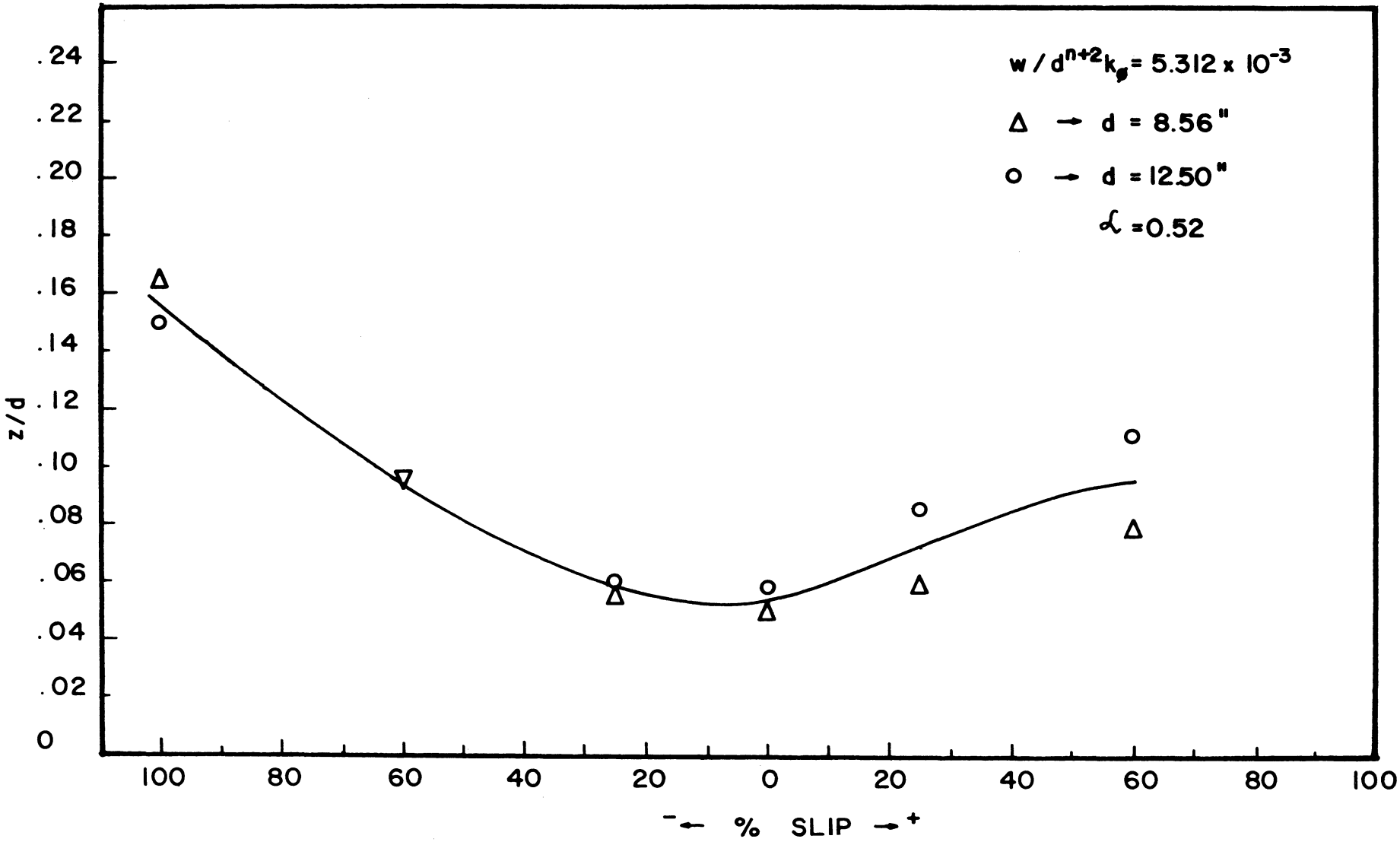

Fig. 18. Plot of (z/d) vs. % slip for ($w/d^{n+2}k_\phi = 5.312 \times 10^{-3}$) under similitude conditions.

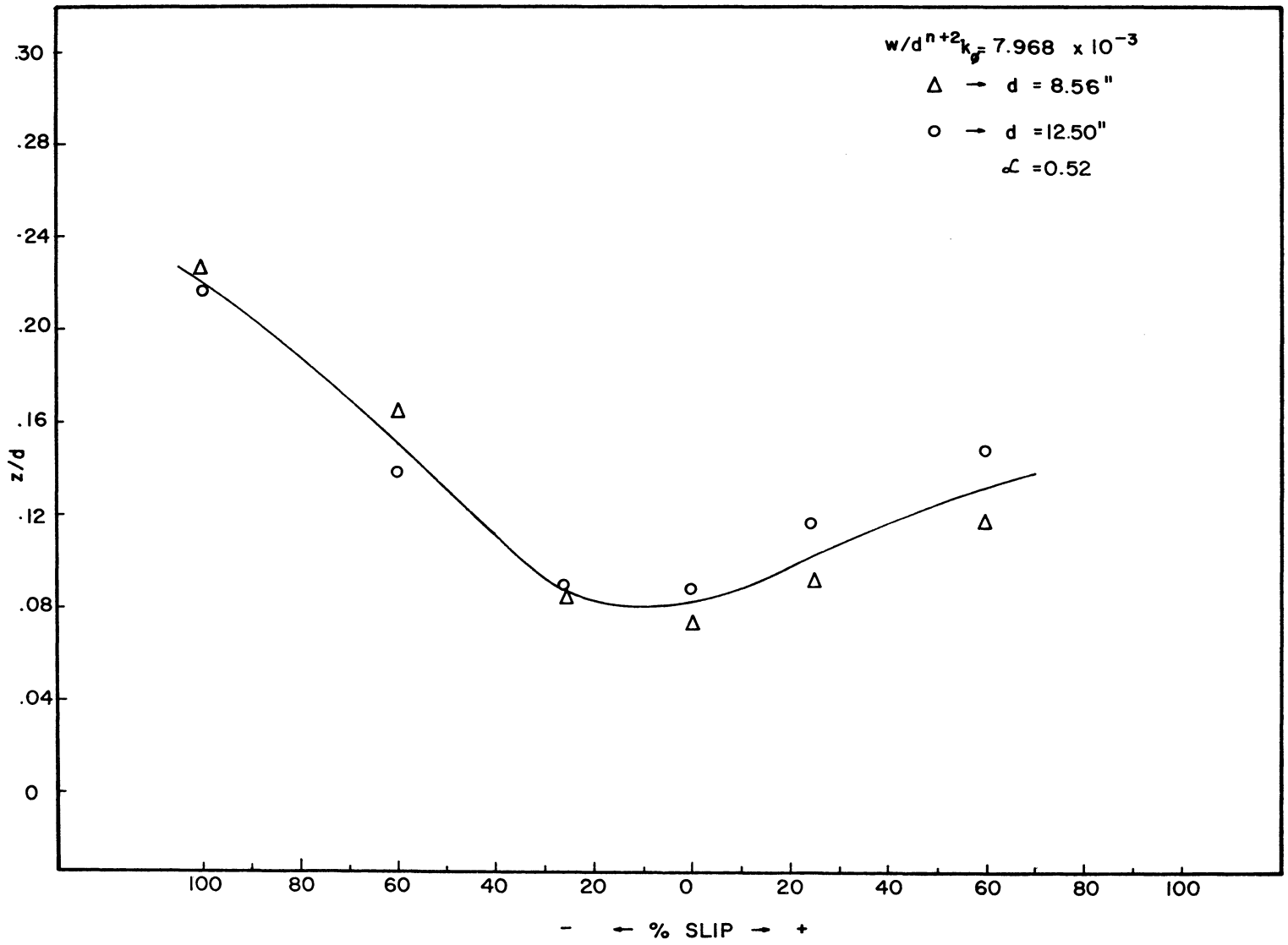

Fig. 19. Plot of (z/d) vs. % slip for ($w/d^{n+2}k_\phi = 7.968 \times 10^{-3}$) under similitude conditions.

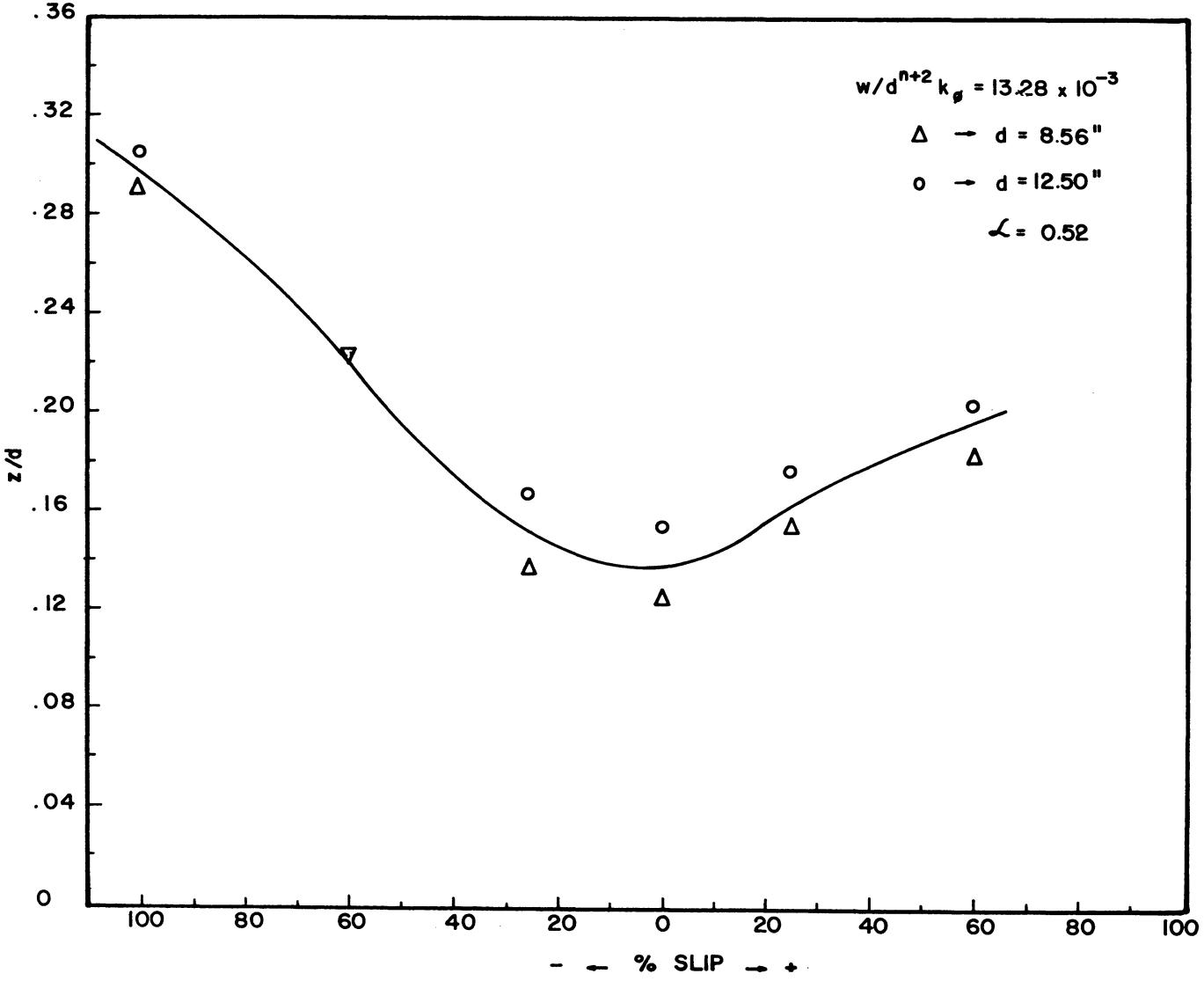

Fig. 20. Plot of (z/d) vs. % slip for ($w/d^{n+2}k_\phi = 13.28 \times 10^{-3}$) under similitude conditions.

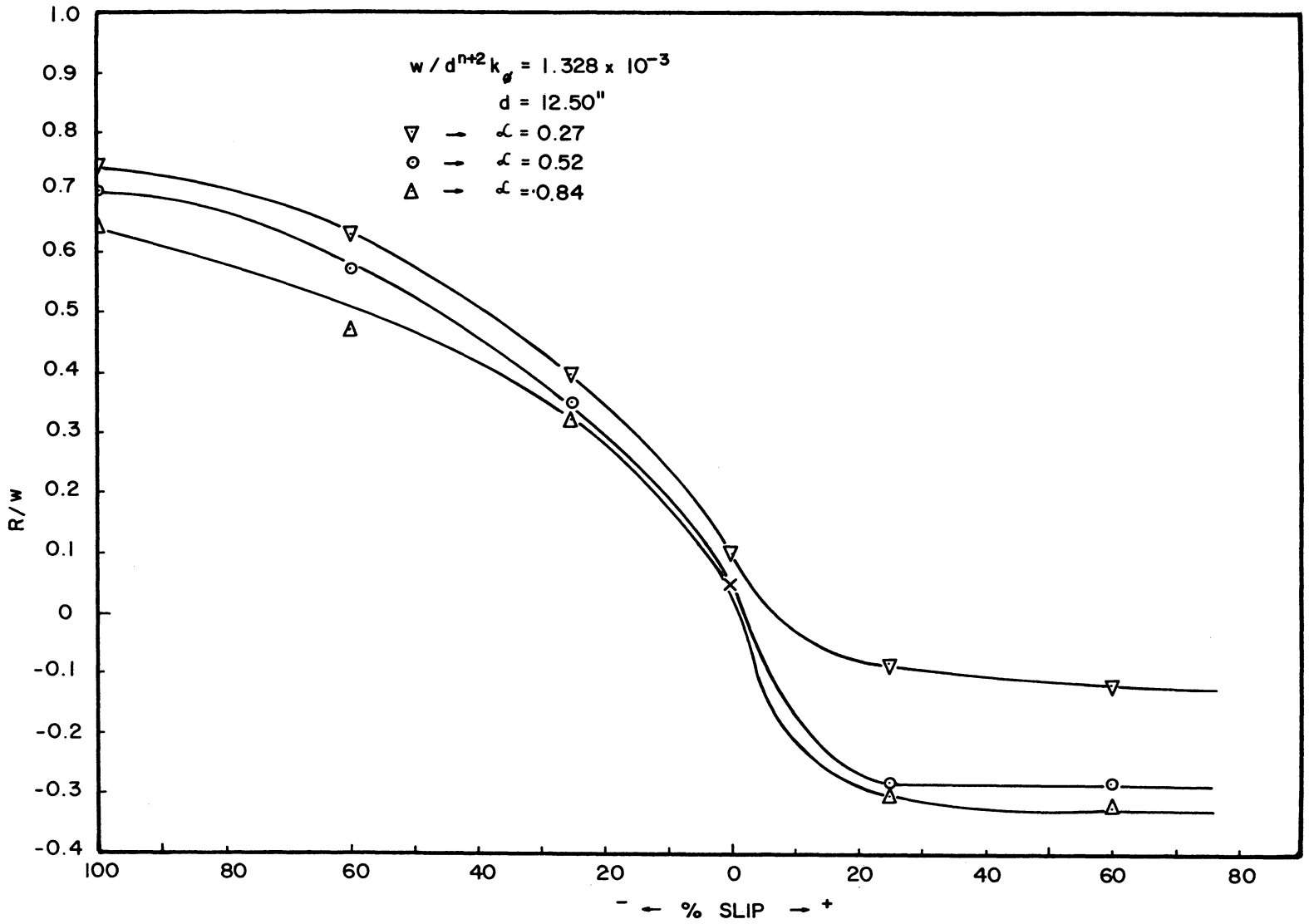

Fig. 21. Plot of (R/w) vs. % slip for ($w/d^{n+2} k_{\phi} = 1.328 \times 10^{-3}$) at various aspect ratios.

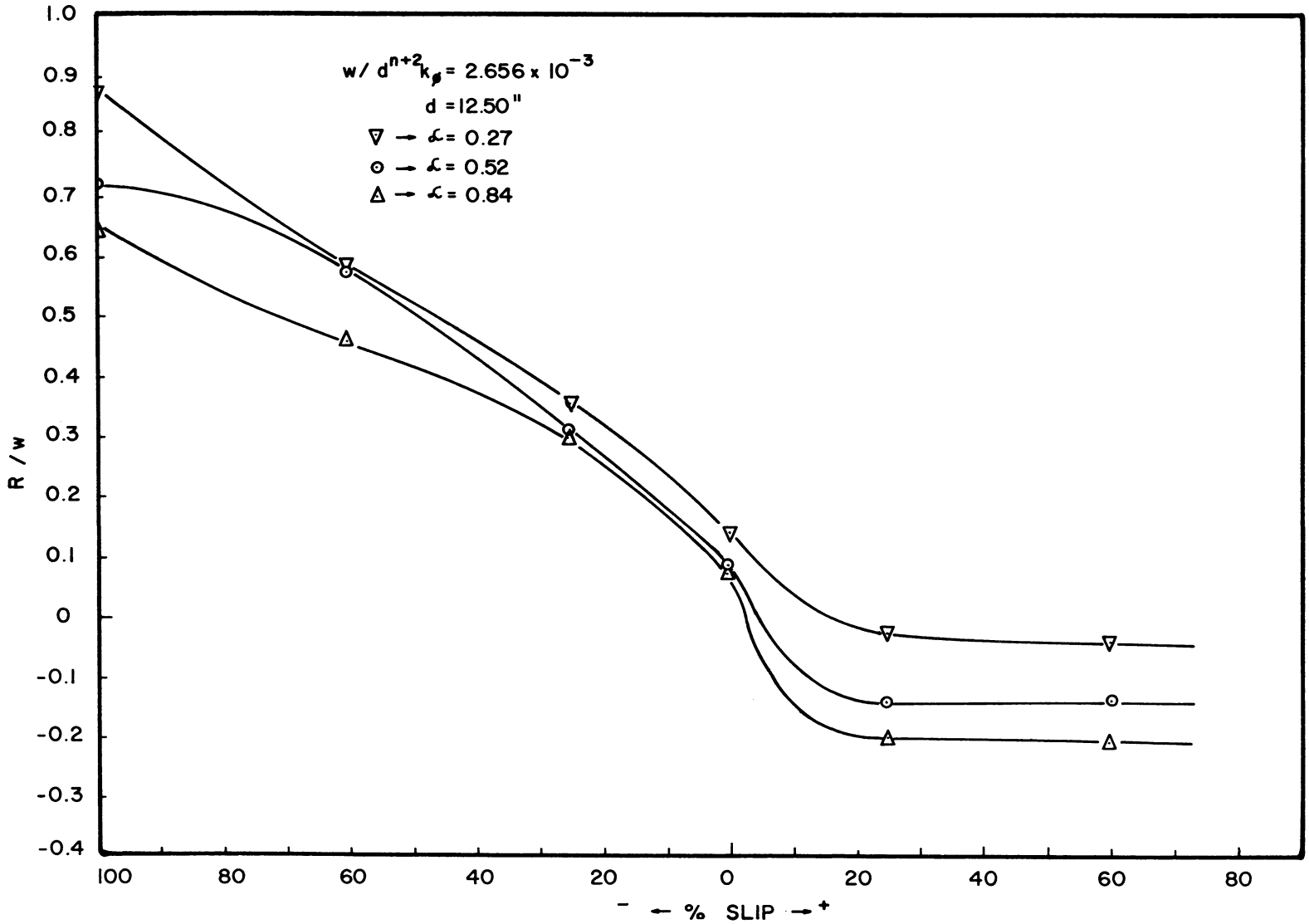

Fig. 22. Plot of (R/w) vs. % slip for ($w/d^{n+2}k_\phi = 2.656 \times 10^{-3}$) at various aspect ratios.

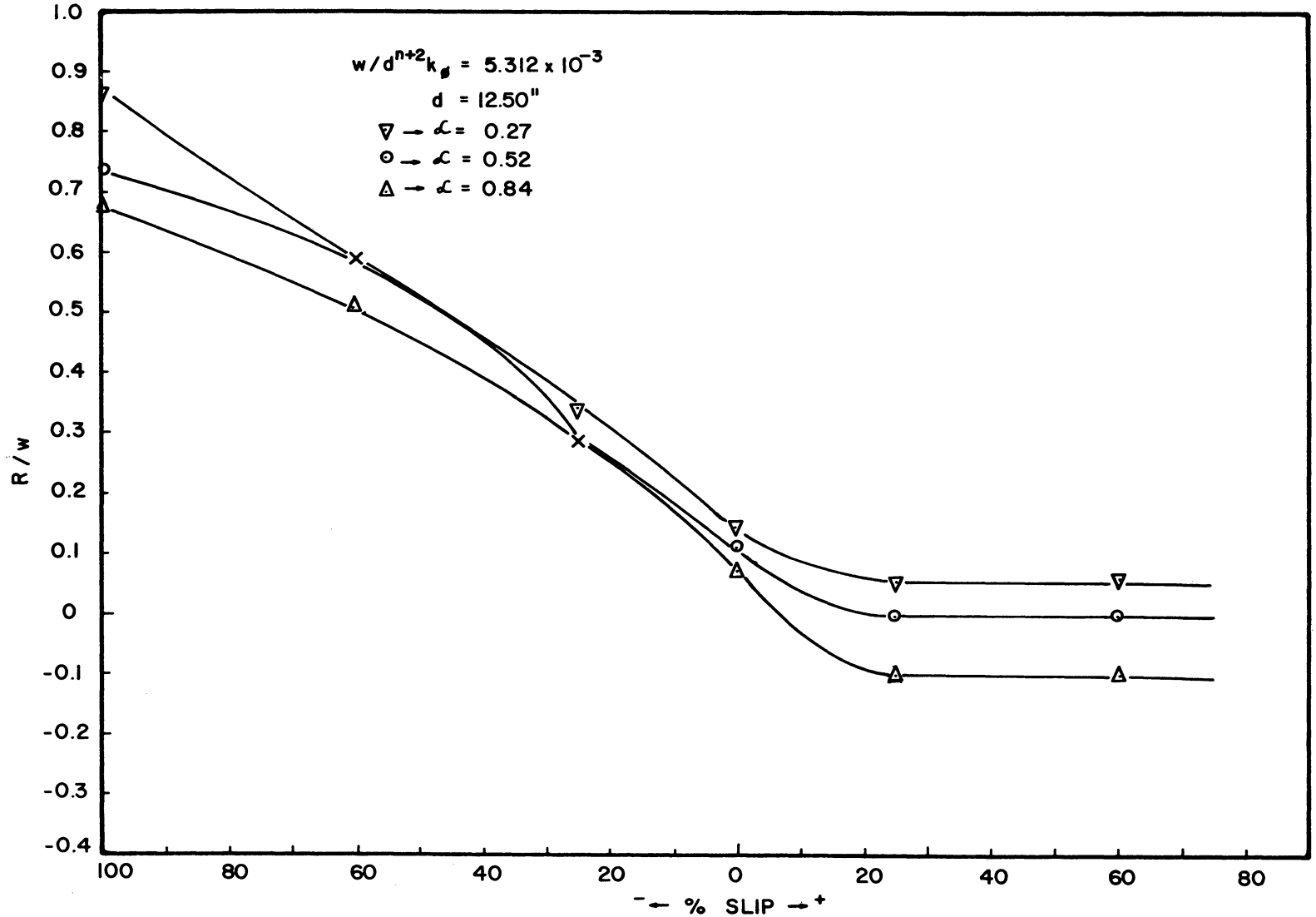

Fig. 23. Plot of (R/w) vs. % slip for ($w/d^{n+2}k_\phi = 5.312 \times 10^{-3}$) at various aspect ratios.

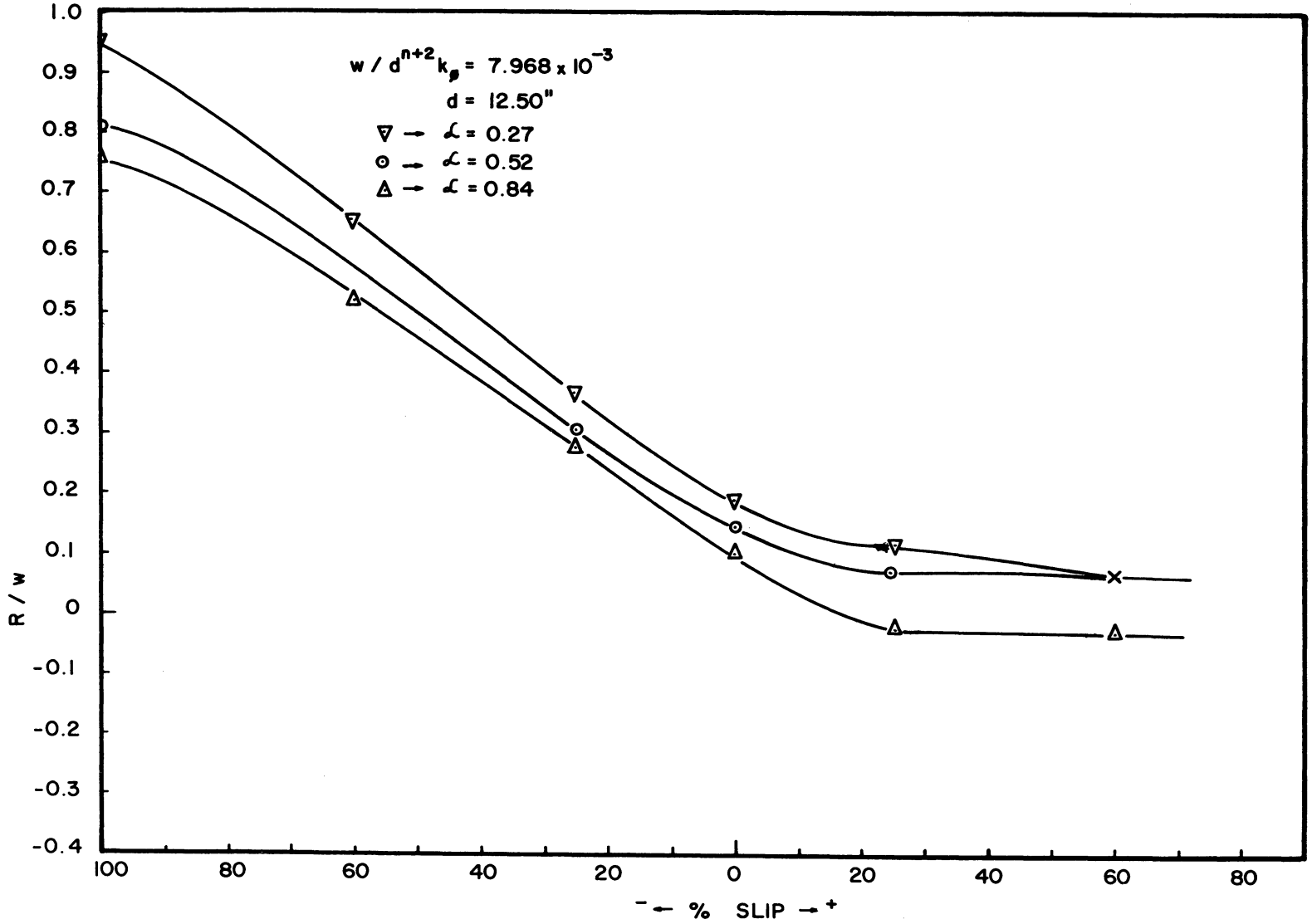

Fig. 24. Plot of (R/w) vs. % slip for ($w/d^{n+2}k_\phi = 7.968 \times 10^{-3}$) at various aspect ratios.

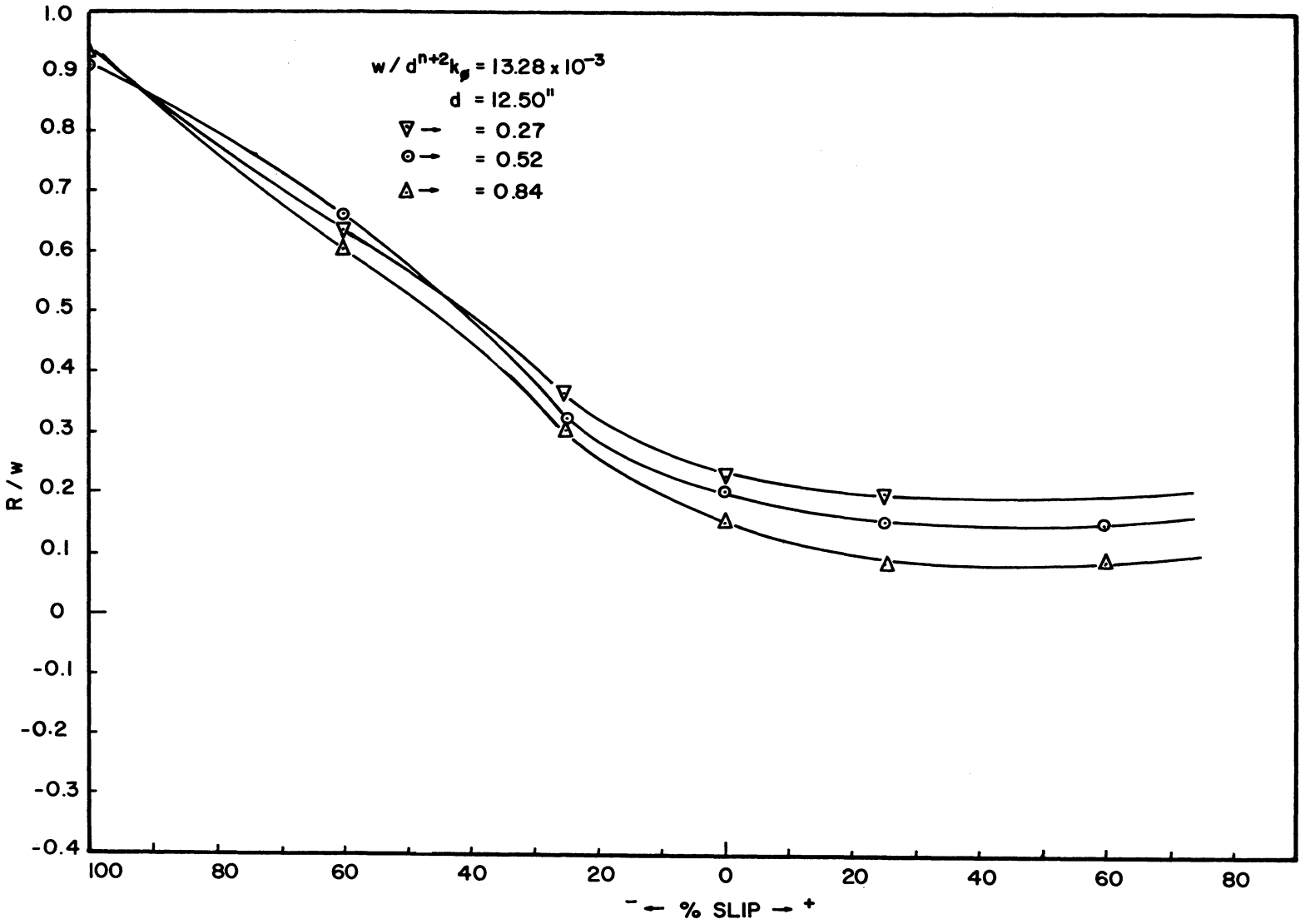

Fig. 25. Plot of (R/w) vs. % slip for ($w/d^{n+2}k_\phi = 13.28 \times 10^{-3}$) at various aspect ratios.

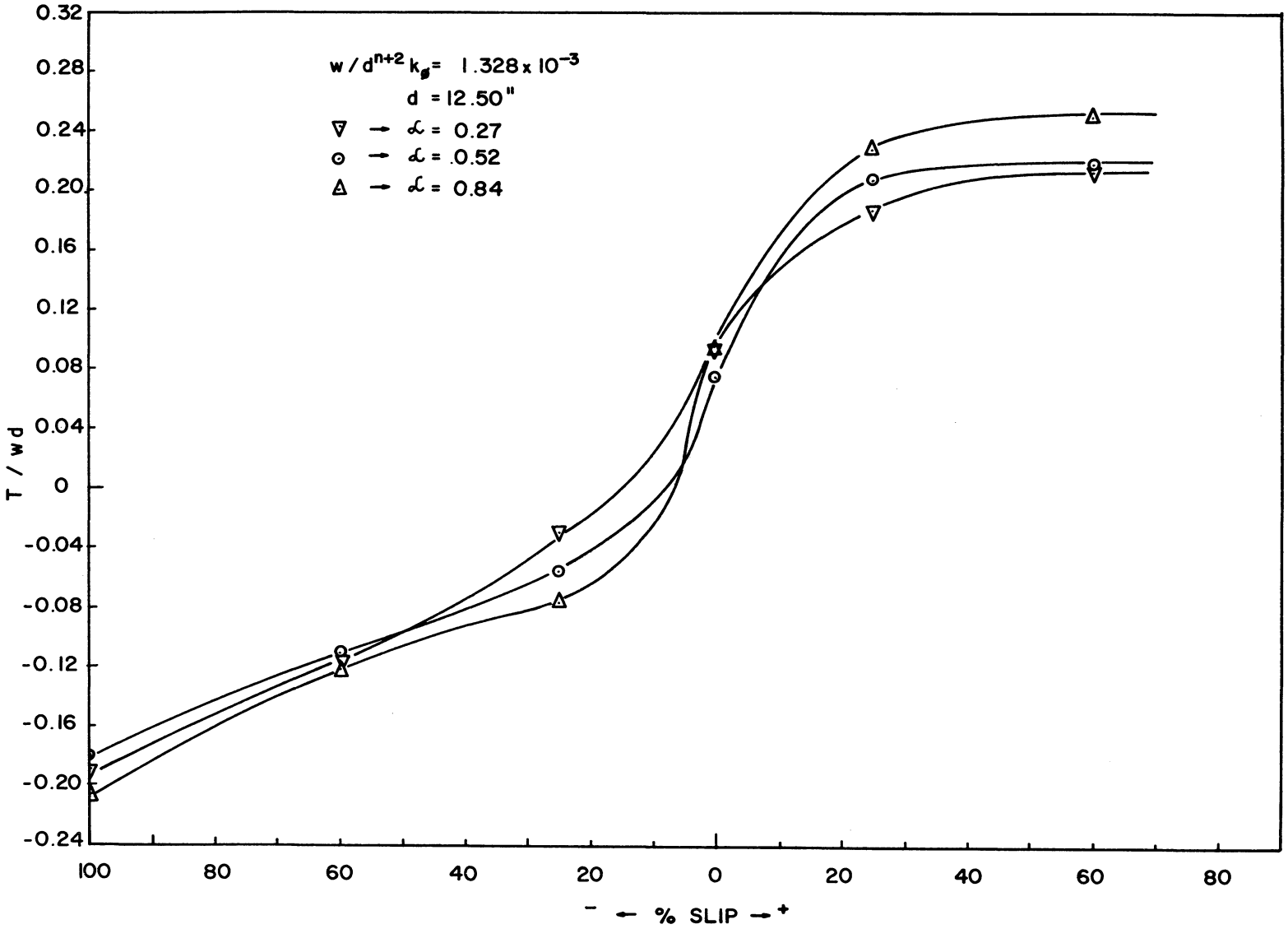

Fig. 26. Plot of (T/wd) vs. % slip for ($w/d^{n+2}k_\phi = 1.328 \times 10^{-3}$) at various aspect ratios.

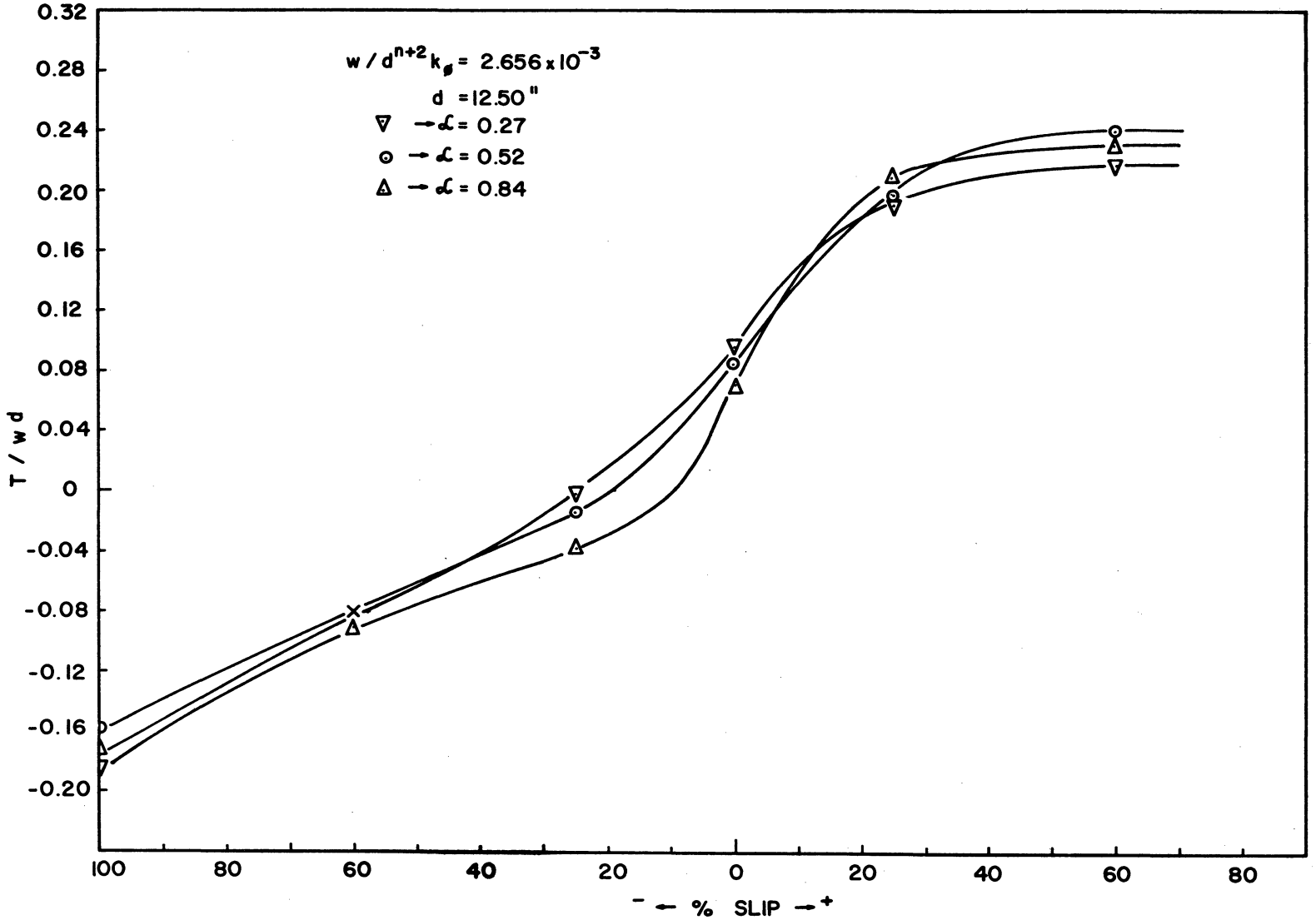

Fig. 27. Plot of (T/wd) vs. % slip for ($w/d^{n+2}k_\phi = 2.656 \times 10^{-3}$) at various aspect ratios.

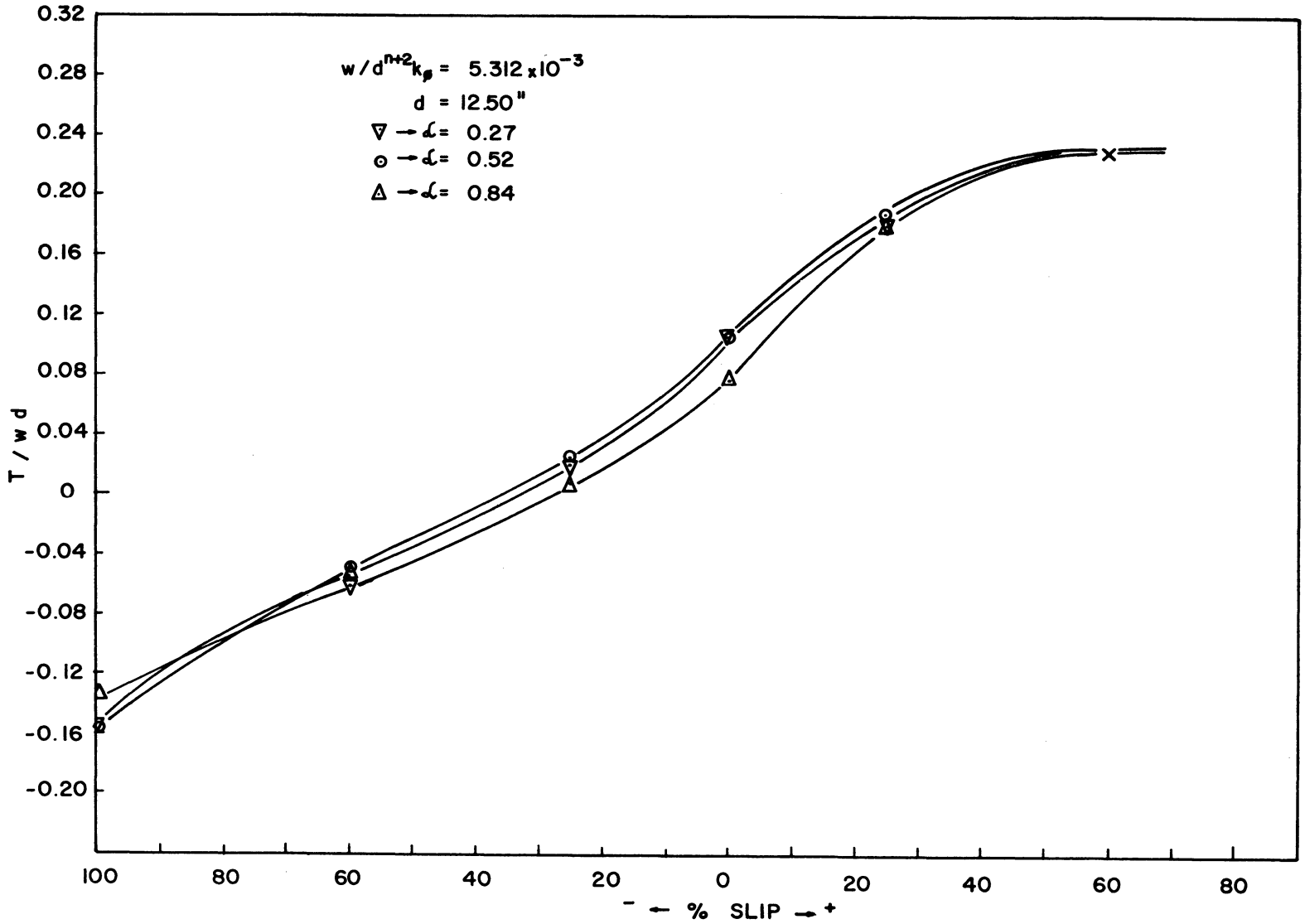

Fig. 28. Plot of (T/wd) vs. % slip for ($w/d^{n+2}k_\phi = 5.312 \times 10^{-3}$) at various aspect ratios.

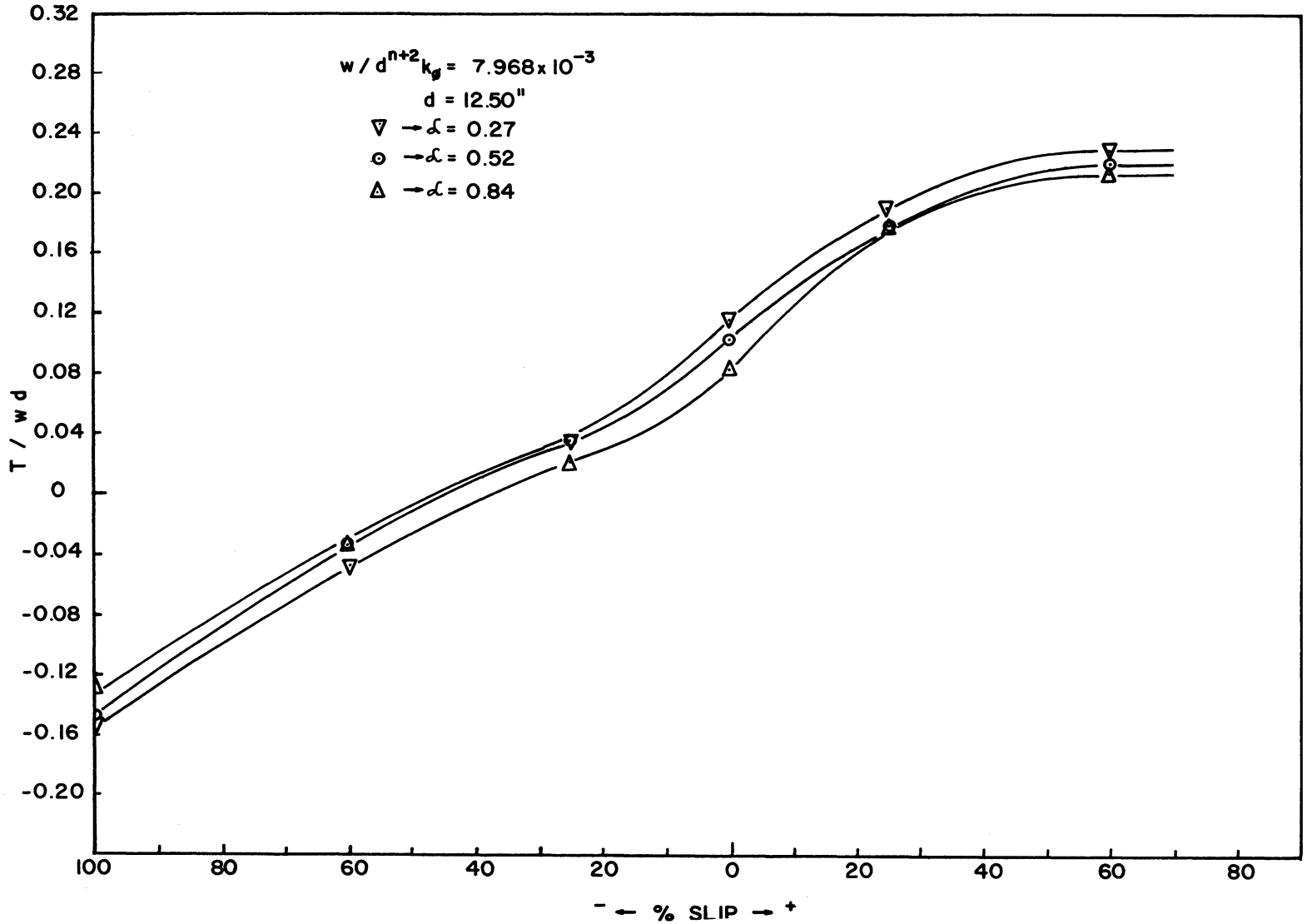

Fig. 29. Plot of (T/wd) vs. % slip for ($w/d^{n+2}k_\phi = 7.968 \times 10^{-3}$) at various aspect ratios.

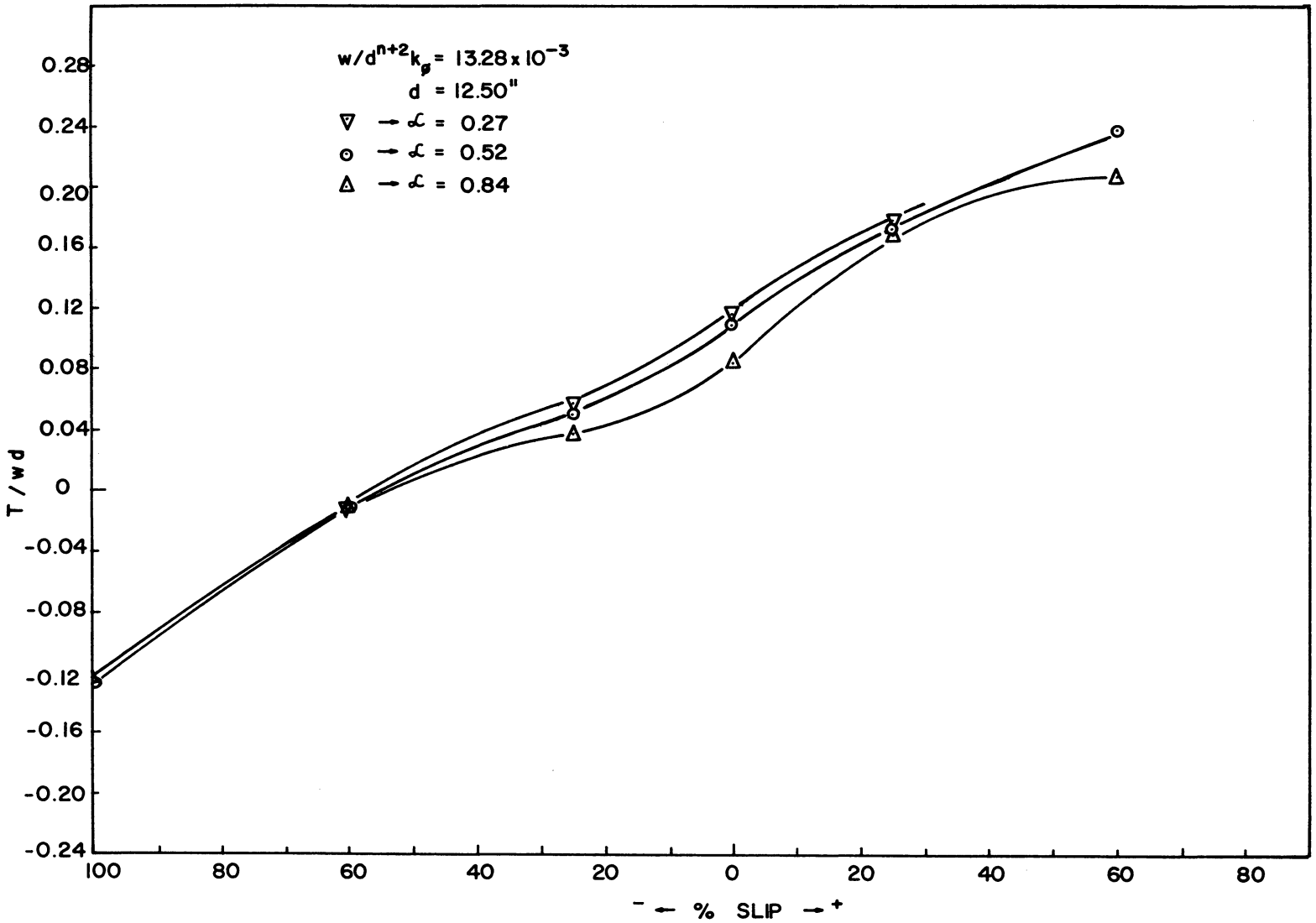

Fig. 30. Plot of (T/wd) vs. % slip for ($w/d^{n+2}k_\phi = 13.28 \times 10^{-3}$) at various aspect ratios.

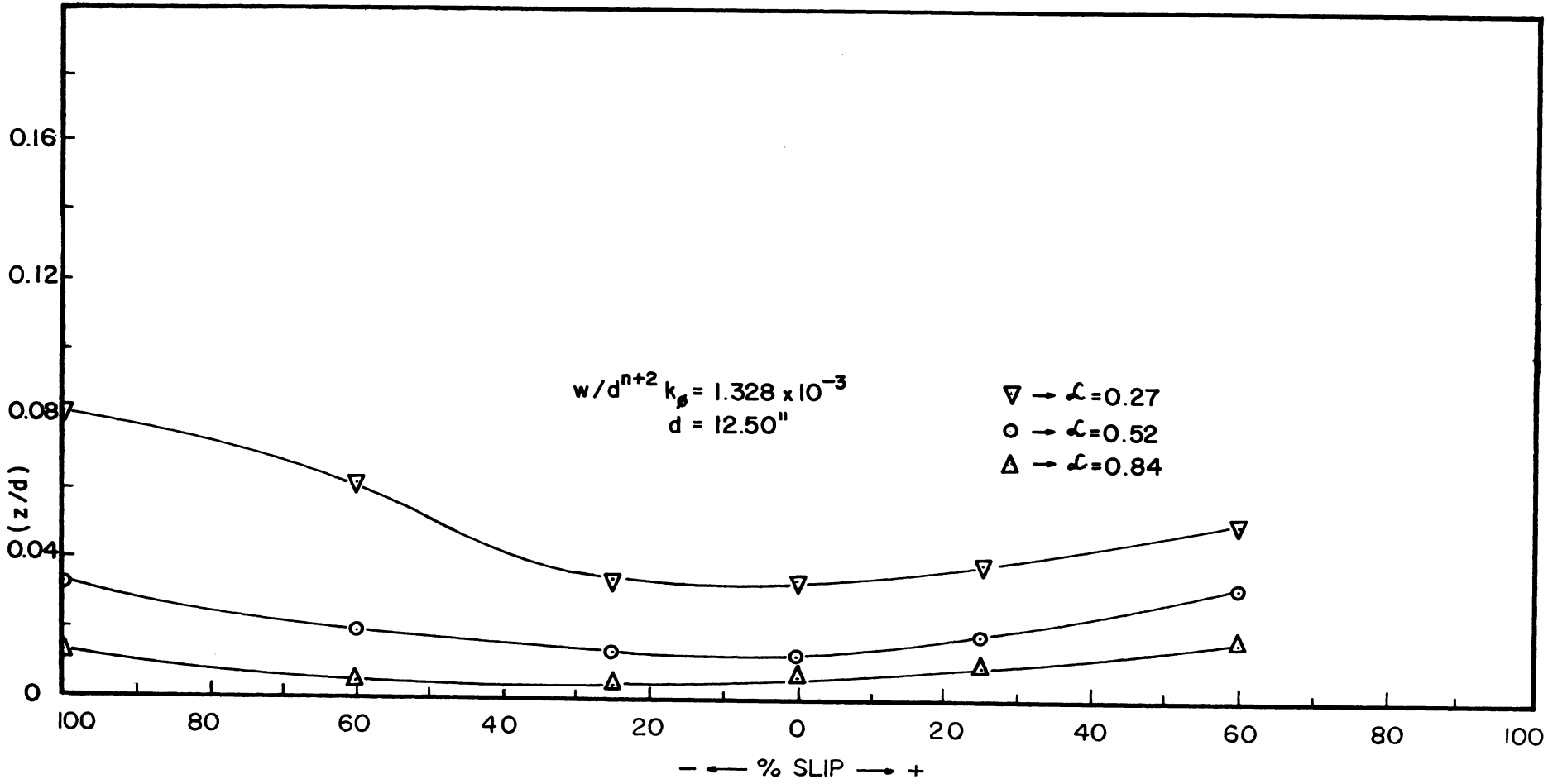

Fig. 31. Plot of (z/d) vs. % slip for ($w/d^{n+2}k_\phi = 1.328 \times 10^{-3}$) at various aspect ratios.

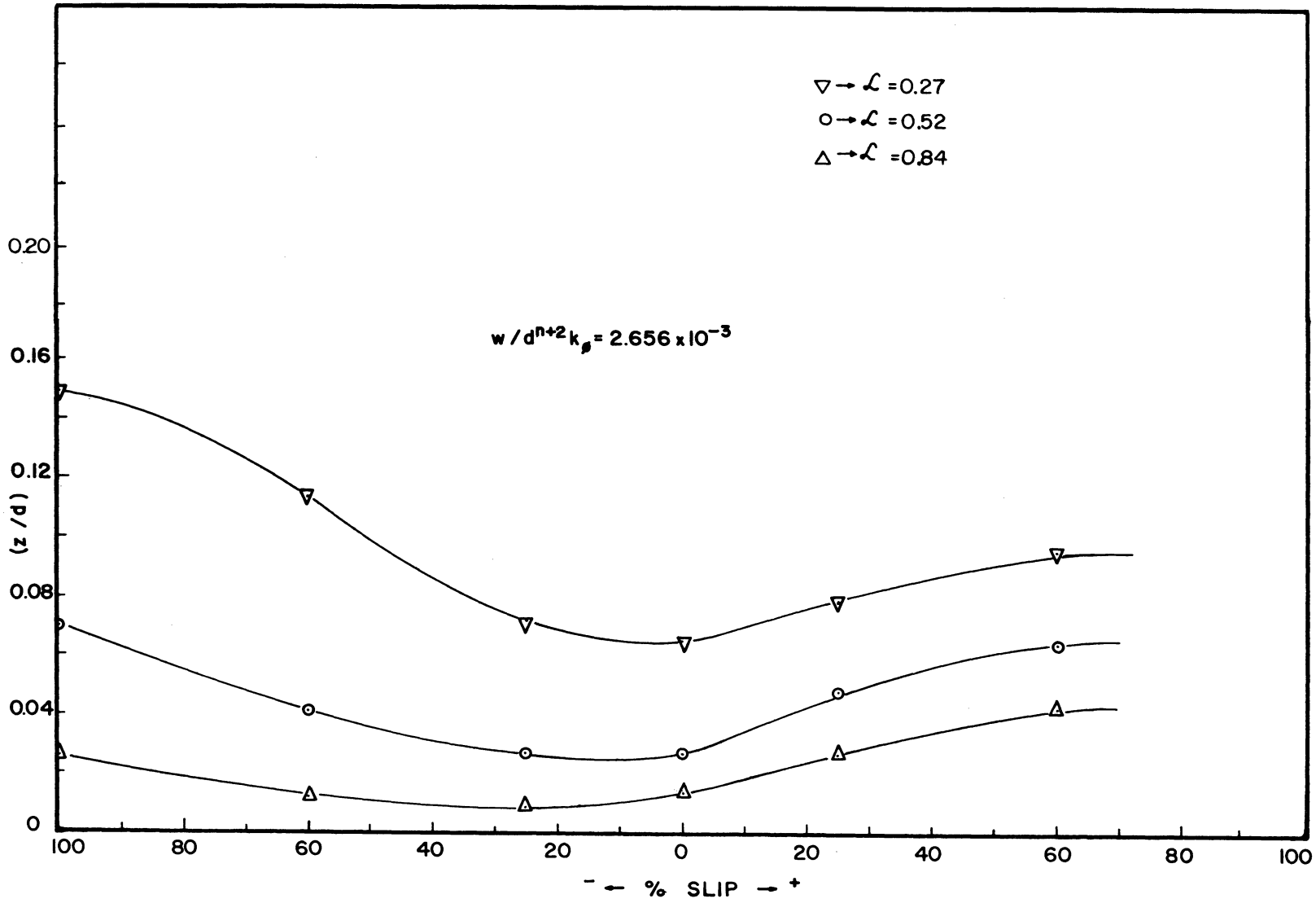

Fig. 32. Plot of (z/d) vs. % slip for ($w/d^{n+2}k_{\phi} = 2.656 \times 10^{-3}$) at various aspect ratios.

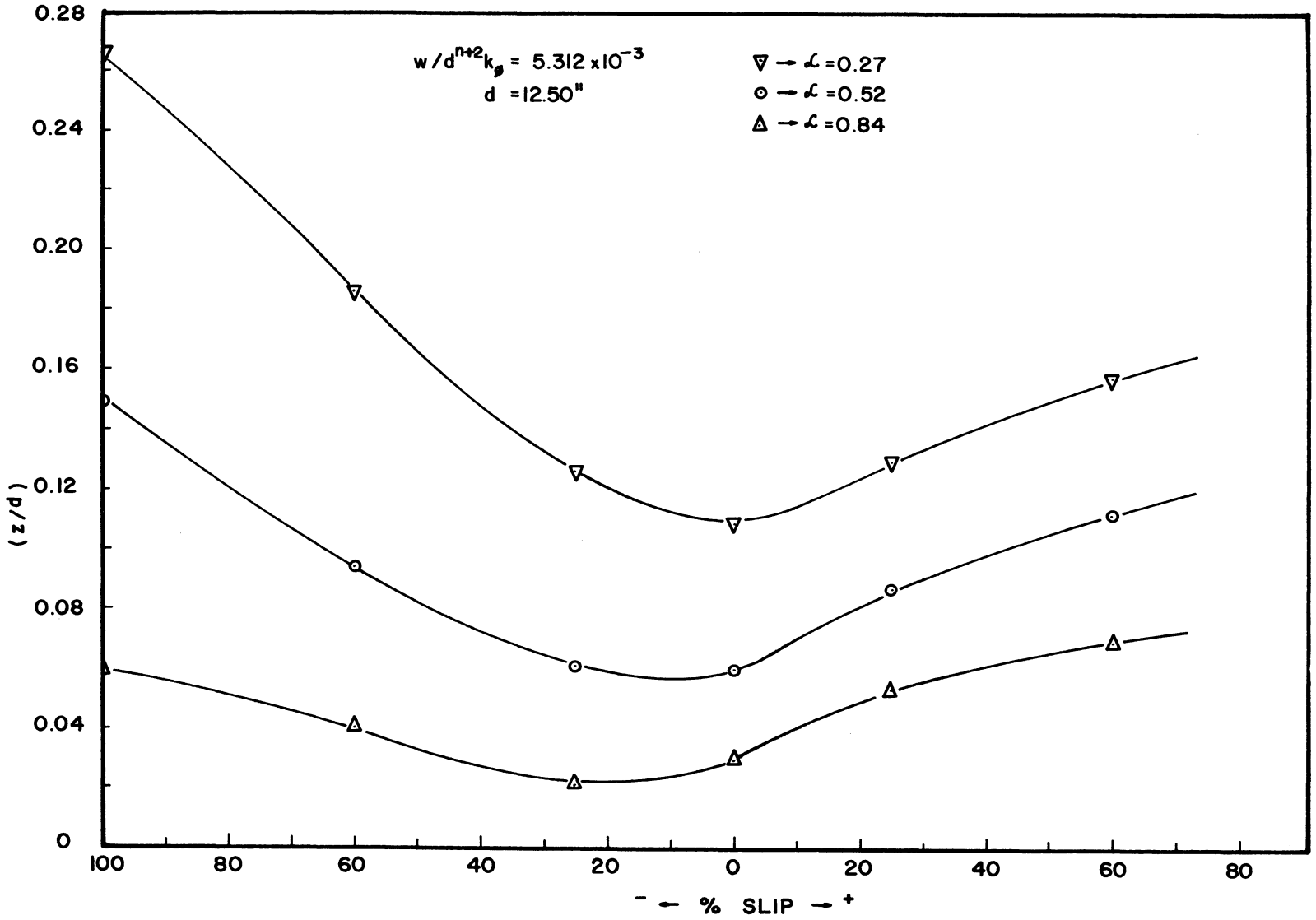

Fig. 33. Plot of (z/d) vs. % slip for ($w/d^{n+2}k_\phi = 5.312 \times 10^{-3}$) at various aspect ratios.

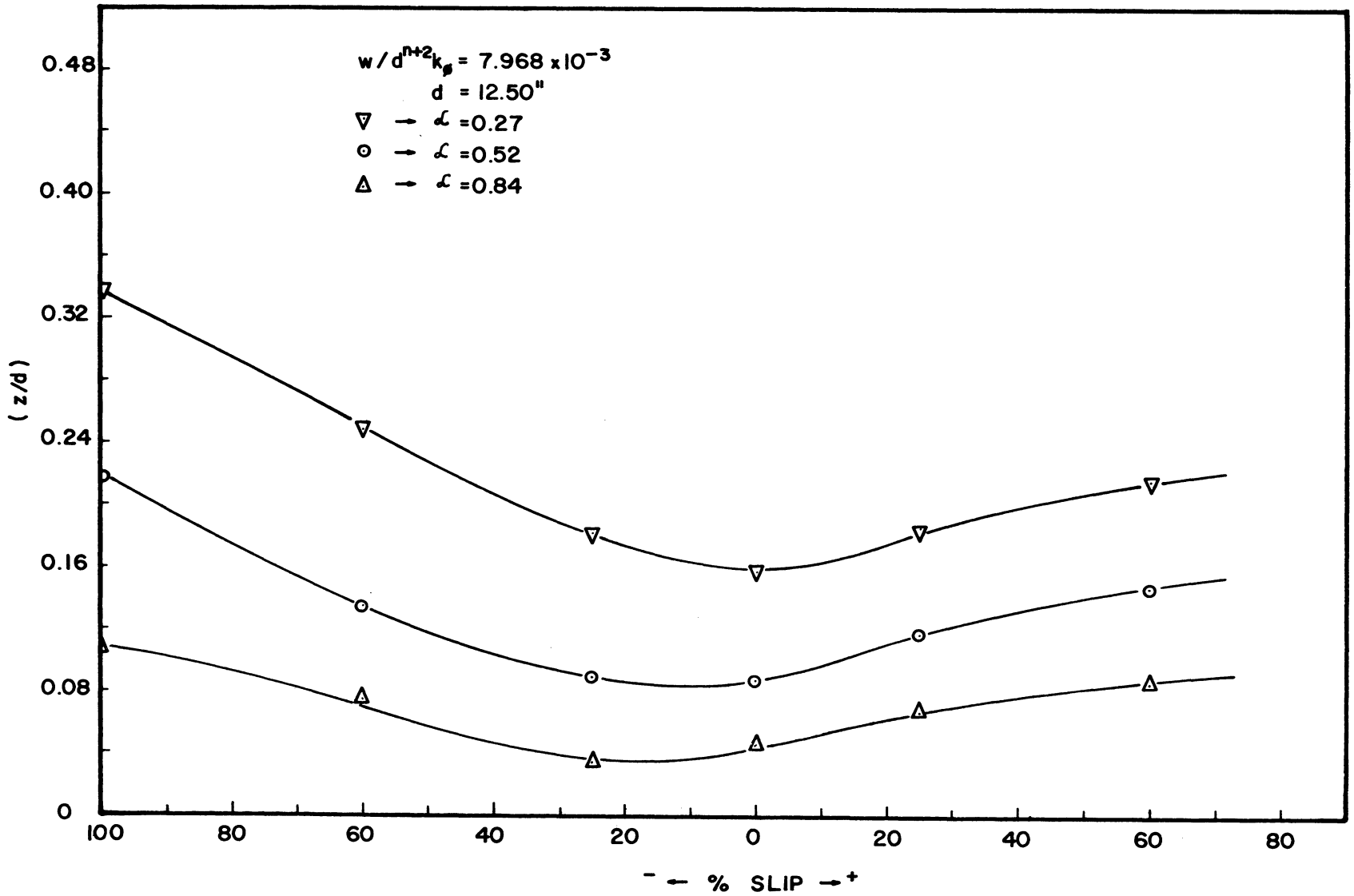

Fig. 34. Plot of (z/d) vs. % slip for ($w/d^{n+2}k_\phi = 7.968 \times 10^{-3}$) at various aspect ratios.

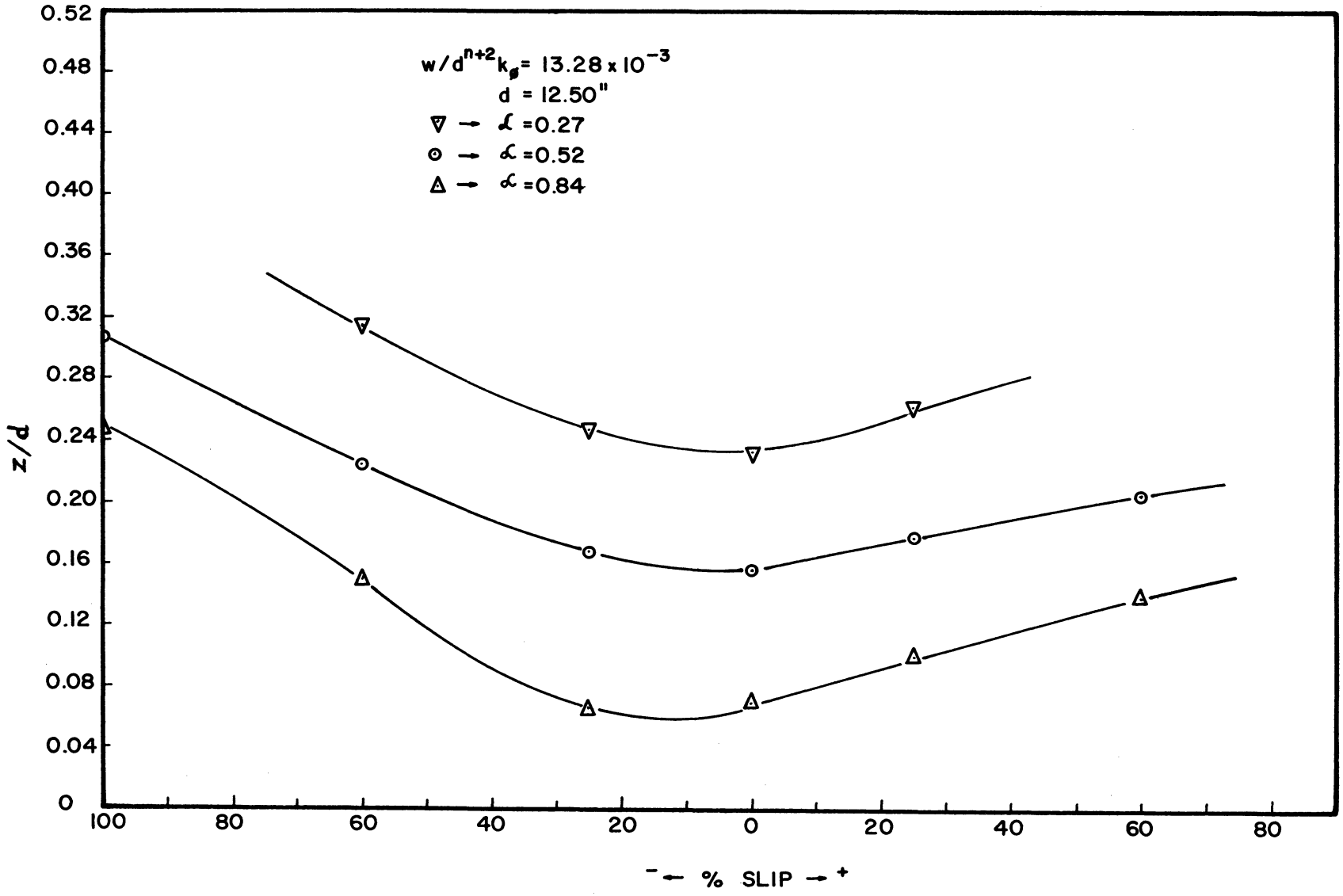

Fig. 35. Plot of (z/d) vs. % slip for ($w/d^{n+2}k_\phi = 13.28 \times 10^{-3}$) at various aspect ratios.

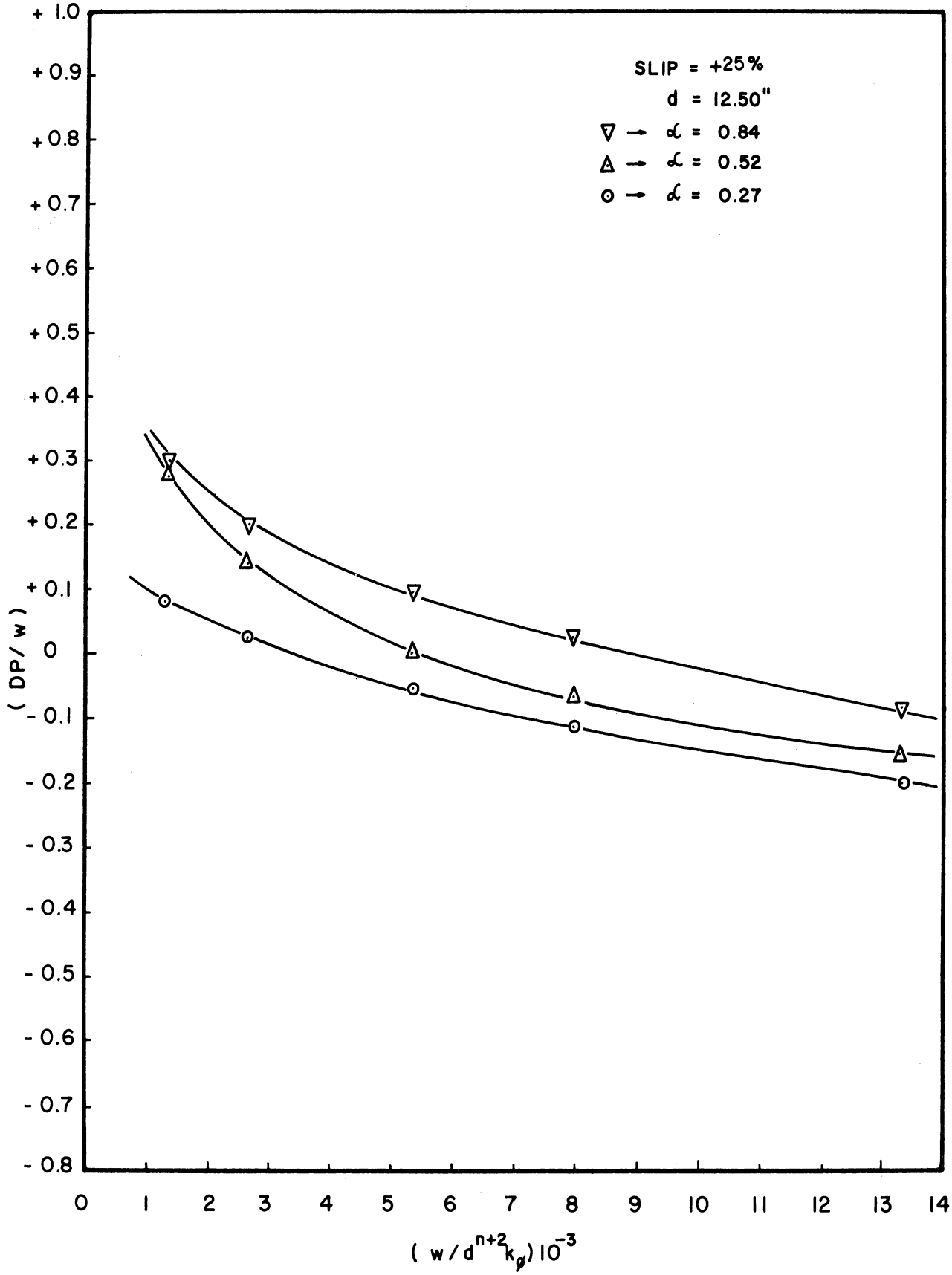

Fig. 36. Plot of (DP/w) vs. $(w/d^{n+2}k_{\phi})10^{-3}$ at +25% slip and various aspect ratios.

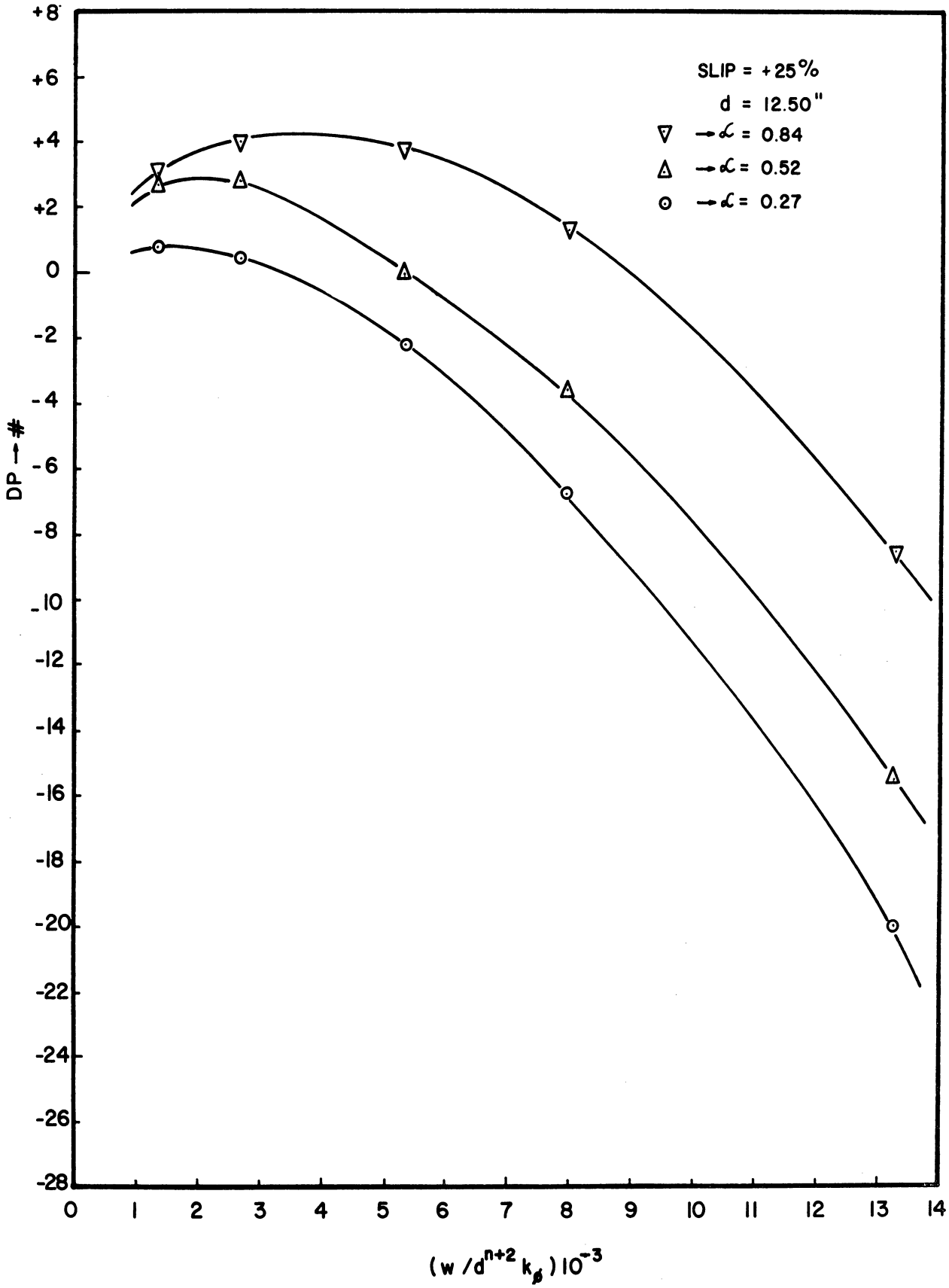

Fig. 37. Plot of DP vs. $(w/d^{n+2}k_{\phi})10^{-3}$ at +25% slip and various aspect ratios.